Ultracold Collision Measurements in Low Intensity Magneto-Optical Traps

by

Renée C. Nesnidal

A dissertation submitted in partial fulfillment

of the requirements for the degree of

Doctor of Philosophy

(Physics)

at the

UNIVERSITY OF WISCONSIN-MADISON

1999

Abstract

I have measured ultracold collision rates for ^{87}Rb in weak magneto-optical traps. This work was motivated by an apparent three order of magnitude discrepancy between two measurements of the ground-state spin exchange collisional loss rate. Standard MOT measurements gave a value of 2×10^{-11} cm^3/s, while a double Bose-condensate experiment gave a rate of $2.2(9)\times10^{-14}$ cm^3/s. The low BEC result was explained by a destructive interference in the singlet and triplet phase shifts, however, the discrepancy between the two results has never been explained. The key result of this thesis is the discovery of an intensity dependence of the trap loss collision rates. At low intensity the collision rate depends linearly on the intensity as opposed to the previously believed intensity independence. A number of possible explanations are presented and analyzed. First, the delicate phase balance that suppressed the rate in the BEC could be disrupted by the presence of the light. Second, the collision could take place as an excited state process. Finally, a flux enhancement process could increase the collision rate.

Acknowledgements

There are so many people who have contributed in some way to this work and to my graduate school experience. I am sure this list is incomplete, and so to anyone who has been left out inadvertently, I apologize. In addition, the people included here have done much more than the few things that I've chosen to mention.

I must, of course, begin by thanking my adviser, Thad Walker. He has certainly had a profound influence on my graduate career as well as in shaping my career goals. Thad's direction and advice has changed my perspective on physics forever.

There are many other Atom Trainers who presence allowed me to accomplish all that I have. Rob Williamson and Paul Feng always took time to stop what they were doing to get me on the right track. They both always tried to make me feel like I belonged in the group. Our post-docs Samir Bali and Charles Sukenik were also very influential. Samir always had a smile and an optimistic perspective. I expect Charles to be ready to work with me in about two weeks. While I've waited for those two weeks, Charles was always available to give me advice and encouragement. Rob, Paul, Samir, and Charles have together taught me almost everything I know about doing experimental physics.

The Atom Trainers who came after me have also been extremely helpful. Steve Kadlecek built several pieces of equipment for me and helped wind the magnetic field coils from hell. His enthusiasm for physics really helped to improve my attitude, espe-

cially when I was feeling less than enthusiastic. Ian Nelson was always there to lend a hand and played a mean guitar in Assault and Broccoli. Other Atom Trainers: Ray Newell, Todd Zimmerman, and Bien Chann made me feel like I knew things by asking questions I knew the answers to. And undergraduate, Russ Hart, gave me the opportunity to be the one to magically fix equipment and gave good advice on movies and books.

Two short-term Atom Trainers but long-time friends, Krista Mullman and Jenny Johnstone Binzley, were also incredibly important to my success in graduate school. Krista provided an infinite amount of moral support and made sure I had a life outside of graduate school. Jenny always knew the right thing to say to make me believe in myself. My roommates for a year, Amanda Goyette and Steve Deiker, made a horrible year a little more bearable.

The office staff in the physics department has been wonderfully helpful. Jean Buehlman, Barb Schutz, Ed Slotten, Jesse Prochaska, Carla Schmidt, Marsha Stanek, Chris Lynch, and Bill Klabunde always made me feel more important than I thought I was. In addition, David Lockman in the mailroom; Walt Wigglesworth and Art Fritsche in the student shop; Art Webb, Jerry Glowacki, and Mike Murray in the electronics shop; and Jim Hanesworth and Bill Grogan with their computer expertise all seemed to actually be interested in my progress in graduate school and in life.

My professors at Lawrence University, David Cook, John Brandenberger, J. Bruce Brackenridge, and John Gastineau through their commitment to excellent teaching fostered my interest in physics. U.W. professors Baha Balantekin and Francis Halzen provided a perfect environment for me to pursue my love of teaching. Prof. Chun Lin proved to me that excellent teachers can be found in research universities (and helped to improve my opera collection).

Of course my biggest cheerleaders throughout graduate school and life have always

been my family. My parents raised me to believe that I could do and succeed at anything. And my sister, Kirsten, always made me feel like my small accomplishments were huge successes. And finally, to my biggest fan, my husband Mike: without you I never would have made it. Even from thousands of miles away you somehow made me feel like I could do this.

Contents

List of Figures

Chapter 1

Introduction

1.1 Overview

In this dissertation I describe ultracold collision experiments that demonstrate an unexpected intensity-dependence of trap loss collisions in weak magneto-optical traps (MOT's). Chapter 2 describes the motivation and background for these experiments. Because typical MOT temperatures are on the order of 100 μK, long-range interactions dominate the collision dynamics. Ultracold collisions are typically measured as a loss of atoms from the trap. Collisions, therefore, are observed only when the energy imparted to the atoms exceeds the trap depth. For moderate trap laser intensity the trap depth is on the order of 1 K. In this intensity regime, the collisions that result in trap loss are excited-state collisions. The two principal mechanisms involving excited state atoms are fine structure changing collisions, whose characteristic energy is equal to the fine structure splitting of ~170K, and radiative redistribution, which provides a continuous range of energies. The trap loss rate due to these excited processes increases with increasing trap laser intensity.

At low trap laser intensity the trap depth can become shallow enough to allow

ground state spin-exchange collisions to escape. Spin exchange collisions occur when two atoms, beginning in the upper hyperfine level of the ground state, interact through the exchange interaction. The exchange interaction becomes important at an interatomic separation of $\sim$ 12 Å, thus spin exchange occurs only at very close range. Through this interaction, one or both of the atoms may change to the lower hyperfine level. Collisions which proceed through this interaction are sometimes referred to as hyperfine-changing collisions. Their characteristic energy is equal to the ground state hyperfine splitting and is approximately 150 mK. A rapid increase in trap loss rate with decreasing intensity in this regime has been attributed to these ground state collisions.[Sesko 89]

Interest in low intensity ultracold collision measurements was motivated by a three order of magnitude discrepancy between ^{87}Rb spin exchange loss rates measured in two different experiments. In 1992, Wallace *et al.* reported trap loss rates in rubidium as a function of trap laser intensity.[Wallace 92] For sufficiently low intensity the trap should become weak enough for all atoms undergoing spin-exchange to escape. Below that point the loss rate was assumed to be independent of intensity. The Wallace data appeared to plateau at a loss rate of 2×10^{-11} cm^3/s

The second measurement of the spin exchange rate was performed using a Bose condensate (BEC). In 1997, Myatt *et al.* successfully condensed two different spin states of ^{87}Rb simultaneously.[Myatt 97] In order to create the double condensate, the elastic collision rate must be much larger than the loss-producing inelastic rate. The inelastic loss process in this case is also spin-exchange collisions. From the MOT measurements as well as theoretical calculations [Tiesinga 91], the spin-exchange rate was assumed to be on the order of 10^{-11} cm^3/s. Under those conditions the double condensate should not be possible. Their experiment was successful, however, and they measured the spin exchange rate to be $2.2(9) \times 10^{-14}$ cm^3/s, nearly three orders of

magnitude smaller than the MOT case.

The very low double condensate spin exchange result was explained theoretically as a destructive interference between the singlet and triplet phase shifts, suppressing the spin exchange mechanism. The destructive interference occurs because the singlet and triplet scattering lengths in ^{87}Rb are nearly identical.[Julienne 97, Burke 97, Kokkelmans 97] Why this suppression does not occur in a MOT was a mystery.

It is not entirely unexpected that the spin-exchange rate for the BEC is smaller than the rate measured with the traditional MOT. An obvious difference between the two measurements is the temperature. The temperature of the BEC was below the 500 nK transition temperature, while MOT temperatures are typically on the order of 100 μK. Williams has theoretically extrapolated the temperature dependence of the spin exchange rate to MOT temperatures. [Williams 98] The maximum rate predicted with these calculations is still a factor of 30 lower than the MOT result.

Because the temperature dependence alone does not adequately account for the difference in loss rates, I have looked at the effect of the presence of the light. BEC experiments are performed in magnetic traps for which there is no light present. In contrast, near resonant laser light is used to create the MOT and is present during the trap loss measurements. Although the ground state collisions would seem to be unaffected by the presence of light, it is possible that light could alter the collision dynamics. For example, interaction with the trapping laser at large interatomic separations could modify the trajectories at close range. To explore the effect that the light has on the collisions, I have measured the trap loss rate as a function of trap laser intensity especially for very weak traps.

Chapter 3 provides a description of the apparatus and the procedure used for taking and analyzing the data. Although the apparatus used for performing these measurements is a standard vapor-loaded magneto-optical trap, there are a few features of the

apparatus that are unique to this experiment. In particular, the background pressure of rubidium must be quite low. To achieve very low background pressure, the vacuum chamber was carefully prepared prior to assembly. In addition to a standard ion pump, a titanium sublimation pump was used to provide increased pumping speed. The pressure in the chamber was below 10^{-11} Torr which allowed trap lifetimes of as long as 1000 seconds. In addition I have improved trap alignment techniques that allow the trap to be operated at much lower intensities than were previously accessible.

To measure the trap loss rate, the MOT was first loaded at high trap laser intensity. Once the trap was loaded, the intensity was reduced to some lower value. The fluorescence from the trapped atoms was recorded as a function of time, and the trap density was measured using a liquid-nitrogen cooled CCD camera. The data were then fit to the analytic solution of the rate equation

$$\frac{dN}{dt} = L - \Gamma N - \beta \int n^2 d^3r, \tag{1.1}$$

where β is the ultracold collision loss rate coefficient, Γ is the loss rate due to collisions with hot background gas atoms and L is the loading rate.

At moderate to high intensities the trap loss rates showed the same trends as those measured in previous experiments. At very low intensity I discovered the remarkable result that the loss rate increases linearly with intensity rather than becoming intensity-independent as was previously predicted. Sample trap loss data is shown in figure 1.1 for a laser detuning of one linewidth and a magnetic field gradient of 18 G/cm.

Chapter 5 provides interpretation and discussion of the results. There are several mechanisms that could provide the observed intensity dependence. One explanation is related to the theoretical work from the double BEC experiment. The basis for the very low spin-exchange rate was a cancellation between the singlet and triplet phase shifts. The presence of the trapping light could mix some of the $1/R^3$ excited state

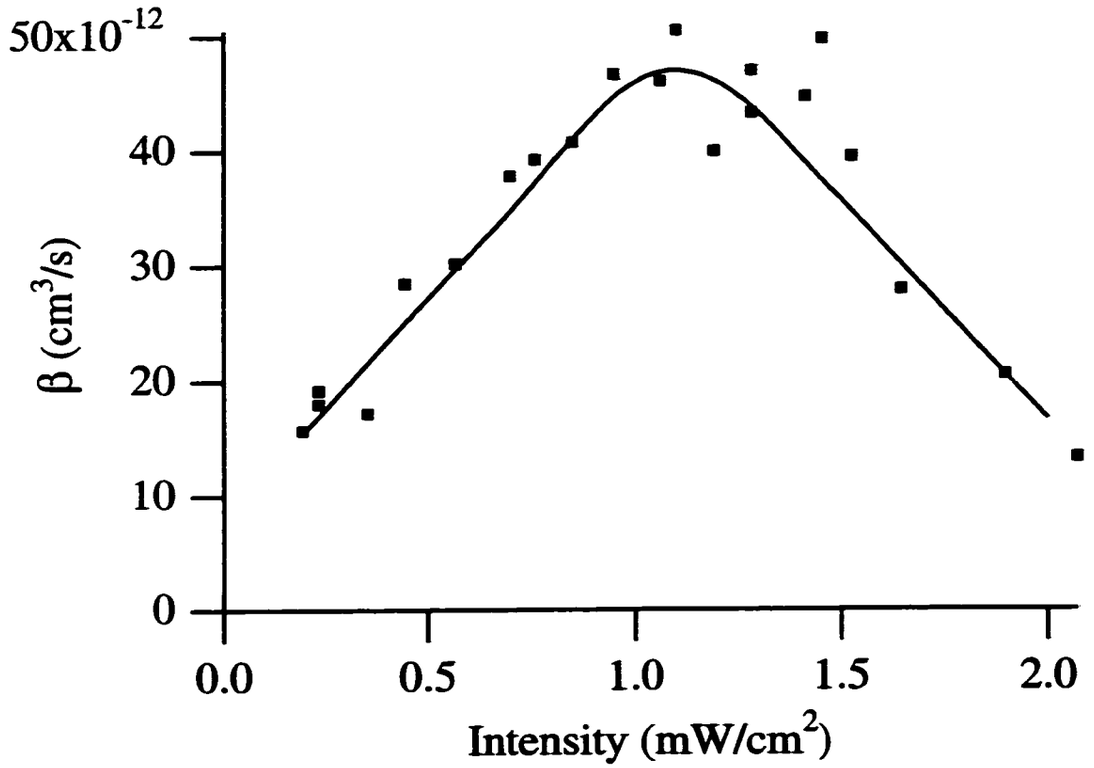

Figure 1.1: Trap loss rate as a function of intensity for $\Delta = -1\Gamma$ and a magnetic field gradient of 18 G/cm. After the increase in loss rate with decreasing intensity, it was previously believed that the loss rate would reach a plateau. Instead the data shows a decrease in loss rate below $\sim$1 mW/cm^2.

potential in with the $1/R^6$ potential. If the singlet and triplet phase shifts are affected differently by the presence of the light, the balance would be disrupted.

Another possible mechanism is an excited state process similar to a fine structure changing collision. The pair could absorb a photon, transferring to an excited potential. Mixing of the potentials could allow a curve crossing to a potential for which the ground state atom changed hyperfine level. Upon radiating to the ground state, the pair would have gained one unit of ground state hyperfine splitting. One characteristic of such a mechanism is that only one atom would change hyperfine levels. A repulsive collision experiment, however, measured the trap depth under conditions comparable to the previous Rb MOT trap loss experiments.[Hoffmann 96] Their measurements indicated that the trap was sufficiently deep that both atoms would have to change hyperfine level in order to escape. Thus an excited state hyperfine changing process is unlikely to be responsible for the measured intensity dependence.

A final mechanism is a flux enhancement process. This process was studied for excited-state collisions and was shown to increase the excited state collisional trap loss rates by a factor of 3.[Sanchez-Villicana 96] The increase is attributed to the fact that the trap laser excites pairs of atoms which are then accelerated on an attractive potential, increasing the flux of atoms reaching close range. I have examined this process classically using a Langevin analysis, for which the loss rate increases by a factor of 2. In terms of angular momentum, the effect of flux enhancement is to allow higher partial waves to overcome the centrifugal barrier. I have examined the effect of additional partial waves on the loss rate. In addition, because the atoms are accelerated, the velocity distributions are modified, and, in particular, the mean velocity is shifted to a larger value. Using the modifed velocity distribution I found an increase in the loss rate by a factor of 2. Furthermore, considering the contributions of higher partial waves I obtained a loss rate of 3.4×10^{-11} cm^3/s. This value is quite close to the peak

observed loss rate of $\sim 5 \times 10^{-11}$ cm^3/s. The inclusion of higher partial waves appears to account for the discrepancy between the MOT measurements and the theoretical rate coefficient including temperature dependence, however, the analysis assumed that all of the atoms were affected by the flux enhancement.

Finally, chapter 6 describes a technique for measuring the excited state fraction for low to moderate intensity traps. This technique was originally developed in order to determine the minimum trap laser intensity required for reliable trap operation. Knowledge of the excited state fraction is important for many experiments involving trapped atoms, however prior to this method the only direct measurement used photoionization out of the excited state.[Dineen 92] The new technique provides a method for determining the saturation intensity which then allows the excited state fraction to be calculated.

1.2 Summary of achievements

I spent the first four years here working on the evanescent project. As a part of that I worked on the design of a multi-layer dielectric structure for enhancing evanescent waves.[Nesnidal 96] The proposed experiment was to drop a sample of trapped atoms onto an evanescent wave and study the ultracold collision dynamics of an atom with its image. One of the novel features of this experiment was that the excited state potential could be tuned because it involved the detuning and strength of the evanescent wave. Thus we could study excited state collisions in which we chose the excited state potential. I also wrote a Monte Carlo simulation for that experiment which was meant to model the distribution of energy that we would see from the atoms after bouncing on the evanescent wave.

After the evanescent wave project, interest turned toward Bose-Einstein conden-

sation. With a BEC experiment in mind, I built and demonstrated loading into a magnetic trap. During that time we were considering possible collision mechanisms to study in the magnetic trap, when we found the interesting discrepancy between the spin exchange rates in BEC as compared to MOT's.

At that point my research turned back to magneto-optical trapping. While attempting to measure trap loss from very weak traps I developed techniques for aligning the lasers and magnetic fields to the tolerances required for very weak traps. In addition I developed a method for measuring the excited state fraction for trapped atoms at moderate laser intensities. While measuring trap loss rates at low trapping intensities, I discovered a new intensity-dependence in the trap loss rate for weak traps.

Chapter 2

Motivation

2.1 Overview

This work has been motivated by two sets of experiments. Section 2.2 describes the standard ultracold collision measurements in magneto-optical traps that first laid the groundwork for the understanding of low-intensity traploss experiments. The following section describes work involving Bose-Einstein condensed atoms. Although the experimental conditions for condensed atoms are different for magneto-optically trapped atoms, in principle the collisional processes are similar. The loss rate due to spin-exchange collisions measured in BEC was three orders of magnitude smaller than the MOT rates, which caused us to speculate on the possible reasons for the difference. The final section considers the differences between the two sets of experiments, temperature and the presence of light. Theoretical calculations showing the temperature dependence do not adequately account for the large discrepancy between the two experiments. Thus we chose to look at the effect of the light on the collision process.

2.2 Ultracold Collision Experiments

Since the demonstration of the first magneto-optical traps [Raab 87], one of the primary research interests has been the study of ultracold collisions. Because of the very low temperatures achieved in MOT's, they provide an interesting arena for studying previously inaccessible physics. Atomic collisions in this regime are unique because of the long interaction times as compared to standard room temperature collisions. The collision time can be much longer than the spontaneous lifetime of the excited state, allowing an atom to absorb and emit photons during the collision. Because the interatomic forces are orders of magnitude different for the ground and excited states, the interaction with photons dominates the collision dynamics. In addition, the role played by long range forces is much larger in ultracold collisions as compared to room temperature collisions.

A common method used for measuring collisions between trapped atoms is to monitor the number of atoms in the trap as a function of time. Ultracold collisions for which the kinetic energy transferred to the atoms is greater than the trap depth are observed as a loss of atoms from the trap. The rate equation describing the density of trapped atoms is given by

$$\frac{dN}{dt} = L - \Gamma N - \beta \int n^2 d^3r, \tag{2.1}$$

where n is the trapped atom density, L is the loading rate in atoms/s, Γ is the loss rate due to collisions with background gas atoms in s^{-1}, and β is the loss rate coefficient due to ultracold collisions in cm^3/s. In the absence of loading, a typical decay is shown in Figure 2.1. The contributions from background collisions and ultracold collisions can be resolved as the density changes in time. The loss rate is first dominated by ultracold collisions, and then at longer times, when the density is significantly smaller,

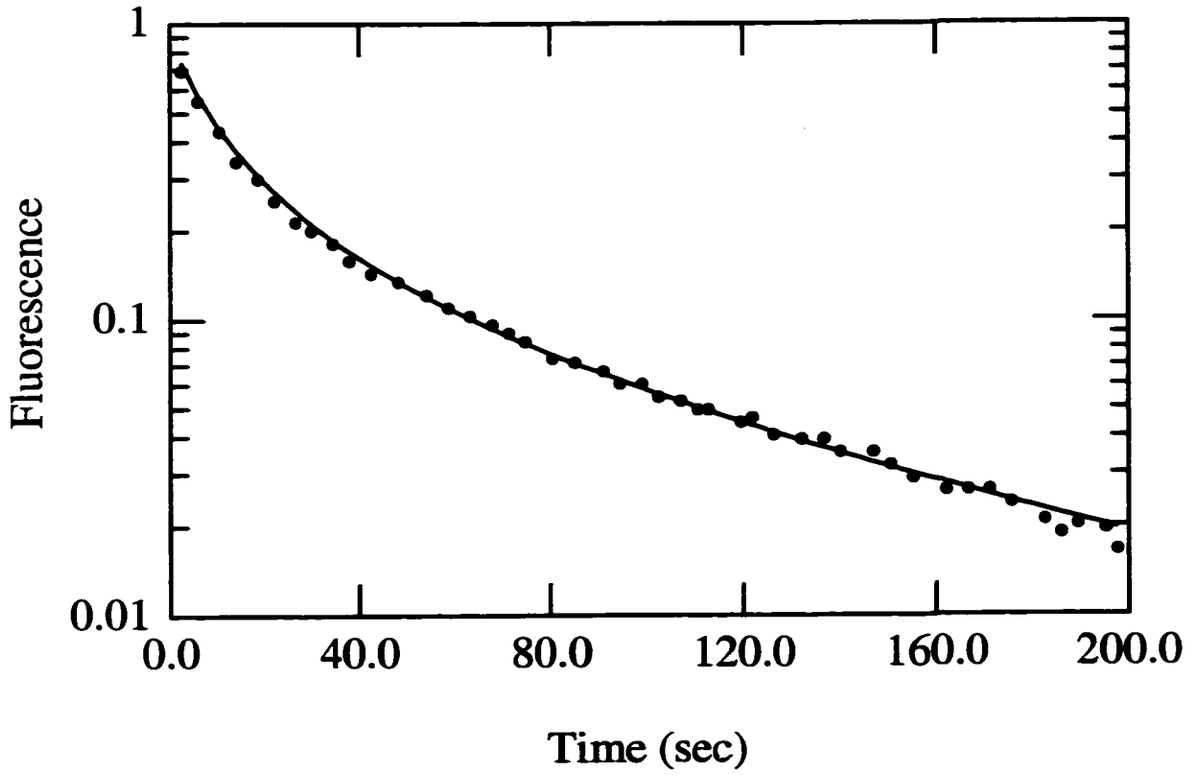

Figure 2.1: Time-dependence of traploss rate without loading. The traploss rate is dominated at first by ultracold collisions when the density is high, after the number of atoms has decreased significantly, the loss due to background collisions dominates.

the loss is dominated by background collisions. On a logarithmic scale, the curvature is due to ultracold collisions while the straight portion is due to background collisions.

Ultracold collisions can be broken down into two basic types: ground state collisions in which both atoms remain in the ground state during the collision, and excited state collisions, in which the atoms absorb a photon during the collision process.

As two ground state atoms collide, at very close range, the exchange interaction, $V_{exch}(\mathbf{S_1} \cdot \mathbf{S_2})$, becomes important. Under the influence of the exchange interaction, one or both of the atoms may change hyperfine level:

$$5^2S_{1/2}(F=2) + 5^2S_{1/2}(F=2) \rightarrow 5^2S_{1/2}(F=1) + 5^2S_{1/2}(F=2) \qquad (2.2)$$

or

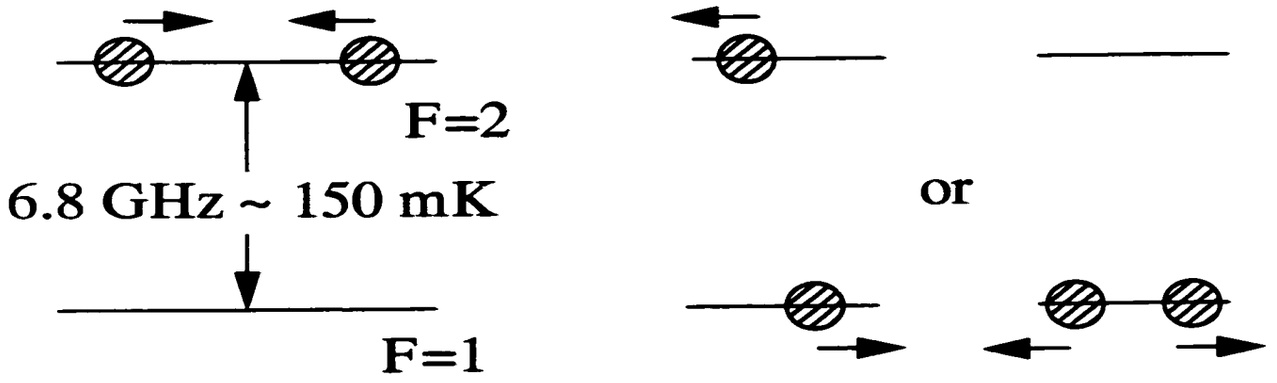

Figure 2.2: Two colliding atoms that both start in the upper hyperfine level can undergo a spin exchange collision in which one or both of the atoms leaves the collision in the lower hyperfine level. The energy gained in such a collision is equal to the ground state hyperfine splitting, 6.83 GHz for ^{87}Rb, for one atom changing hyperfine level or 13.66 GHz if both change.

$$\rightarrow \quad 5^2S_{1/2}(F=1) + 5^2S_{1/2}(F=1) \qquad (2.3)$$

As shown in figure 2.2, the kinetic energy acquired by the atoms in the first case is equal to the ground state hyperfine splitting, and in the second case the kinetic energy is twice the hyperfine splitting. The ground state hyperfine splitting for ^{87}Rb is 6.83 GHz which corresponds to a temperature of approximately 150mK. Because of the small energy acquired, atoms undergoing hyperfine changing collisions can only escape very weak traps.

On the other hand, excited state trap loss collisions are believed to occur via two main mechanisms, fine-structure changing collisions and radiative escape. Both mechanisms are illustrated in Figure 2.3. In a fine structure changing collision, after absorbing a photon tuned near the $5S_{1/2} - 5P_{3/2}$ state, the atoms are accelerated toward one another on the $5S_{1/2} + 5P_{3/2}$ molecular potential. Due to mixing of the $5P_{3/2}$ and $5P_{1/2}$ potentials, if the atoms survive on the excited state potential to very small interatomic separation they can undergo a fine-structure changing collision:

$$5^2S_{1/2} + 5^2P_{3/2} \rightarrow 5^2S_{1/2} + 5^2P_{1/2} \qquad (2.4)$$

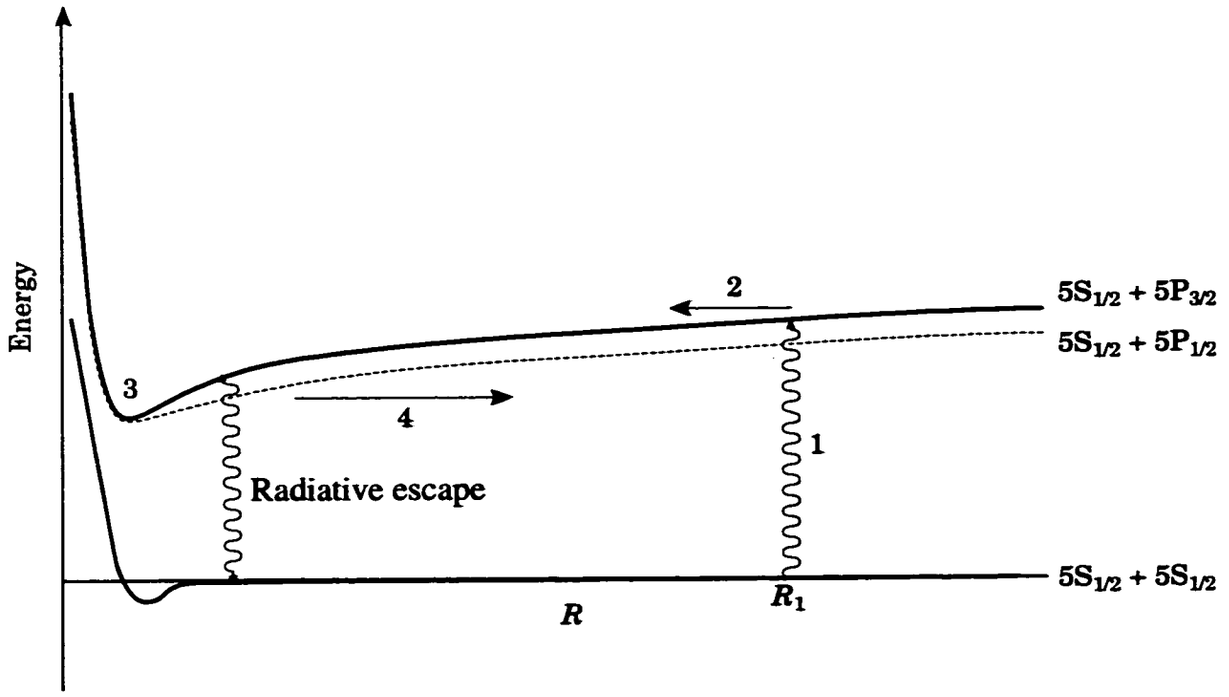

Figure 2.3: Mechanisms for excited state collisional trap loss. In both processes, one atom absorbs a photon at separation R_1. The atoms are accelerated toward each other on the $5S_{1/2} + 5P_{3/2}$ molecular potential. Radiative escape occurs when a less energetic photon is emitted when the atoms are a fairly close range. A fine-structure changing collision occurs when the atoms get close enough to undergo a curve crossing with the $5S_{1/2} + 5P_{1/2}$, acquiring kinetic energy equal to the fine structure splitting.

Under this circumstance the atoms gain kinetic energy equal to the fine structure splitting. For ^{87}Rb this splitting is on the order of 170K,which greatly exceeds the trap depth.

The second type of excited-state collision is radiative escape, also called radiative redistribution. Again, during the collision an atom absorbs a photon and the collision proceeds on the excited molecular potential. After the atoms acquire an energy greater than the trap depth, they radiate to the ground state. Due to the attractive nature of the potential, the photon emitted by the colliding pair is less energetic than the initially absorbed photon. Because the atoms tend to radiate to unbound states, radiative escape provides a continuous range of energies to the atoms in contrast to fine-structure changing collisions in which a discrete amount of energy is imparted.

The first set of experiments that motivated our work were studies of the intensity dependence of traploss rates in alkali MOT's. In 1989, Sesko *et al.* measured the intensity dependence of traploss for cesium.[Sesko 89] Their measured loss rate as a function of intensity is shown in figure 2.4. In their work, they identified two different regimes for traploss due to ultracold collisions. At high intensity the trap loss rate increases with increasing intensity. In that regime the trap loss mechanism is dominated by excited state collisions. As the trap laser intensity is decreased, the loss rate decreases until it reaches a minimum whereupon the loss rate increases sharply. The rapid increase at low intensity was interpreted as an indication that the trap depth had become too weak to confine atoms that had acquired the ~ 0.1 K energy imparted in spin exchange collisions.

In 1992, Wallace *et al.* at the University of Connecticut extended the ultracold collision studies to rubidium. The traploss rates as a function of intensity showed the same shape as the data of Sesko *et al.* In addition, they observed significantly different behavior between the two isotopes, ^{85}Rb and ^{87}Rb. At high intensities they found that

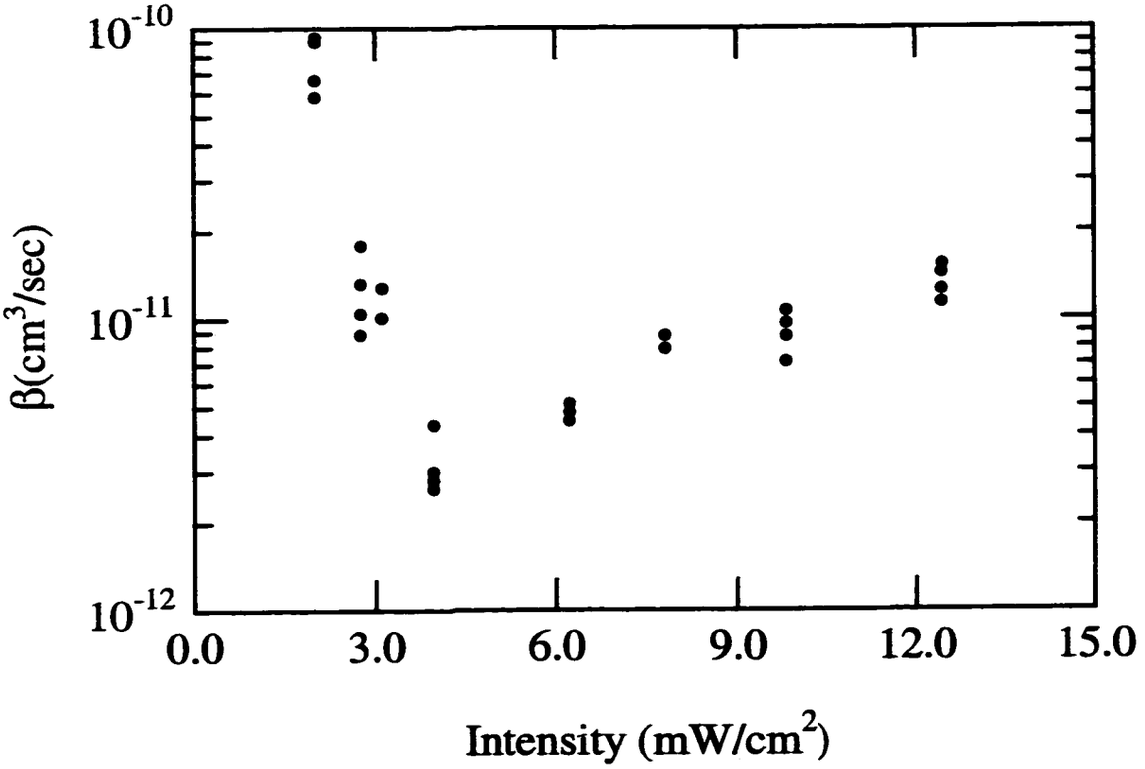

Figure 2.4: Traploss as a function of trap laser intensity for Cs. The rapid increase in loss rate with decreasing intensity has been interpreted as an indication that ground state spin exchange collisions could escape the trap.[Sesko 89]

the loss rate for ^{85}Rb was consistently a factor of 3.3 larger than for ^{87}Rb, which they attributed to differences in the ground and excited state hyperfine structure between the two isotopes. In addition the loss rate at low intensities began to increase with decreasing intensity at a higher intensity for ^{87}Rb than ^{85}Rb. Again, because the ground state hyperfine splitting is approximately twice as large in ^{87}Rb as compared to ^{85}Rb, the energy released in a spin-exchange collision will be twice as large for ^{87}Rb. Thus a larger trap depth is required to confine spin-exchange products in ^{87}Rb. Although the two isotopes showed different behaviors, they found that β leveled off at roughly the same value for both isotopes, 2×10^{-11} cm^3/s. They noted that the turn on of the hyperfine changing collision channel was sloped because the trap was not perfectly isotropic. As the rate begins to increase, loss is allowed only in the least damped direction, and the leveling off was interpreted as the point at which escape was allowed in all directions.

In 1997 the Connecticut group published a more complete study of the intensity dependence for both isotopes of rubidium over a range of trap laser detunings.[Gensemer 97] Their results were consistent with the 1992 data, and the ^{87}Rb results are shown in figure 2.5. In addition they provided further evidence that the sharp increase in the loss rate is due to hyperfine changing collisions. To show that the effect was due to atoms leaving the collision in the lower ground state, they attenuated the hyperfine pumping laser. Attenuation of the repumping laser allows atoms in the lower, untrapped hyperfine level to travel farther before being repumped into the trapped level. They were able to attenuate the hyperfine pumping intensity by a factor of four without seeing any change in the traploss rate, however, for increased attenuation they observed a sudden increase in the loss rate. The properties of the trap such as volume and excited state fraction were unaffected by attenuations up to a factor of 10. Thus at least one of the atoms undergoing this collision process must find itself in the lower hyperfine

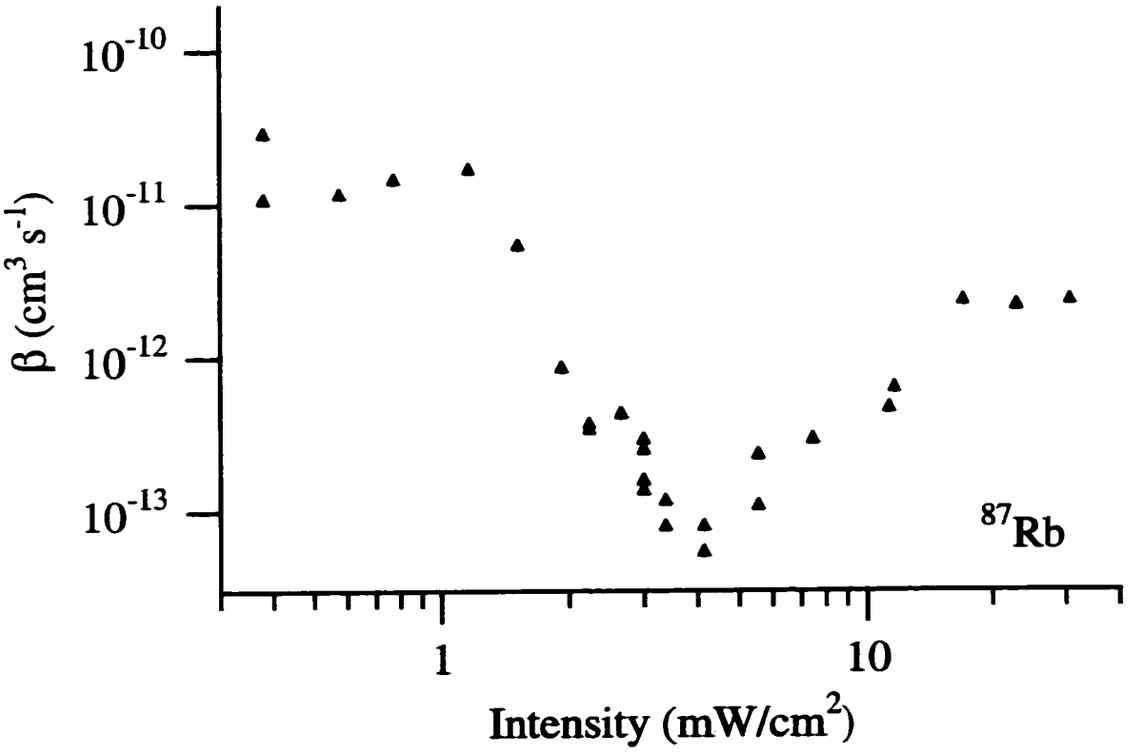

Figure 2.5: Traploss as a function of trap laser intensity for ^{87}Rb measured by [Gensemer 97]. Again the increase in loss rate with decreasing intensity has been attributed to spin exchange collisions. In addition, the apparent plateau at the lowest intensities was interpreted as an indication that the loss rate due to spin exchange was intensity independent.

level.

The low intensity behavior of the trap loss rate is quite suggestive of spin exchange collisions. The intensity for which loss rate begins to increase with decreasing intensity is consistent with the trap depth becoming shallow enough for spin exchange products to escape the trap. Furthermore, the measurements of trap loss as a function of hyperfine pumping intensity show that the atoms are in fact ending up in the lower hyperfine level. The apparent leveling off of the trap loss rate at very low intensities also suggests that the trap can no longer recapture spin exchange products, indicating that the spin exchange rate is 2×10^{-11} cm^3/s.

2.3 Double Bose Condensate

A more recent advance in atomic physics was the experimental observation of Bose-Einstein condensation (BEC) in dilute gases. [Anderson 95, Bradley 95, Davis 95] BEC has provided yet another arena for studying ultracold atoms. The procedure for achieving a sample of condensed atoms begins with a MOT. The atoms are then transferred to a magnetic trap and are cooled through evaporative cooling. In that process the confining potential is lowered to allow the most energetic atoms to leave the sample. The remaining atoms then rethermalize to a lower temperature. This process is continued until the atoms reach the transition temperature to condense.

In 1997 the group at Colorado successfully created a double Bose condensate, consisting of two different spin states of ^{87}Rb, $|F=1, m=-1\rangle$ and $|F=2, m=2\rangle$.[Myatt 97] The $|F=1,m=-1\rangle$ atoms were evaporatively cooled as in a standard Bose condensation experiments. The other state, however, was cooled sympathetically through elastic collisions with the evaporatively cooled atoms. Sympathetic cooling has the advantage that it produces much lower loss rates as compared with the inherently high loss asso-

ciated with evaporative cooling. One potential application for sympathetic cooling is the production of degenerate Fermi gases.

In order for the sympathetic cooling to take place efficiently, the elastic collision rate must be large compared to the inelastic rate. The MOT measurement of 2×10^{-11} cm^3/s suggested that the dominant inelastic loss mechanism, spin exchange collisions should be prohibitively large. In addition, the theoretical predictions at the time of the experiment also predicted the rate to be on the order of 10^{-11} cm^3/s.[Tiesinga 91] Despite predictions, the double condensate was achieved. Measurement of the densities of the two species as well as the loss rates gave a total rate constant of $2.2(9) \times 10^{-14} cm^3/s$, some three orders of magnitude smaller than the measurements made with MOT's.

The theoretical basis for the low spin-exchange rate was found to be caused by a fortuitous matching of the singlet and triplet scattering lengths in ^{87}Rb.[Kokkelmans 97, Julienne 97, Burke 97] Large uncertainty in the rubidium scattering lengths had made previous theoretical predictions of the rate coefficients very difficult. The extremely low observed rate provided the necessary limitations on the scattering lengths to improve the theoretical understanding. The cross-section for spin-exchange collisions is proportional to $\sin^2(\phi_s - \phi_t)$, where $\phi_{s,t}$ are the singlet and triplet phase shifts. The phase shifts are related to the scattering lengths by $\phi_{s,t} = \frac{-ka_{s,t}}{1+k^2a_{s,t}^2}$.* The close matching of the scattering lengths provides destructive interference between those terms, suppressing the spin-exchange collisions. Prior to the double condensate result, the possibility of a cancellation between the singlet and triplet phases had not been considered. The fortuitous matching of scattering lengths appears to exist only for rubidium, and thus this cancellation is not expected to be observed in the other alkalis.

*This formula should not be taken too seriously as it predicts a cancellation in the cross-section at 190μK.

Prior to creation of the double condensate, rubidium scattering length measurements had very large uncertainty. The measured spin exchange rate of $2.2(9)\times10^{-14}$ cm^3/s has led to an improved theoretical understanding of the scattering length for ^{87}Rb. In addition, the three order of magnitude discrepancy as compared to the MOT measurements has led us to believe that there must be more to understand about the spin exchange collisions.

2.4 Connecting the MOT and BEC Results

This three order of magnitude discrepancy between the MOT and BEC measurements of the spin exchange rate seemed to be indicative of interesting physics. Although the two experiments are quite different, the loss process is supposedly identical. The obvious differences between the experiments are the large difference in temperature,$100\mu K$ for MOT's and 500nK for BEC, and the presence of near-resonant light in the MOT.

Carl Williams has theoretically modelled the temperature dependence of the spin-exchange process using a full configuration interaction calculation using the best available potentials.[Williams 98] The double condensate experiment imposed tight restrictions on the singlet and triplet scattering lengths. These improved scattering length values were then used to further impose stringent limitations on the boundary conditions for calculating the spin-exchange cross sections. The results of these calculations are shown in Figure 2.6. In addition to the theoretical predictions, the experimentally determined rate coefficients for the MOT and the double BEC experiments are shown at the appropriate temperatures. Even allowing the MOT temperature to be at the position of the maximum predicted rate, the measured rate would still be approximately a factor of 30 too high. Clearly the temperature dependence alone does not account for the difference between the two rates.

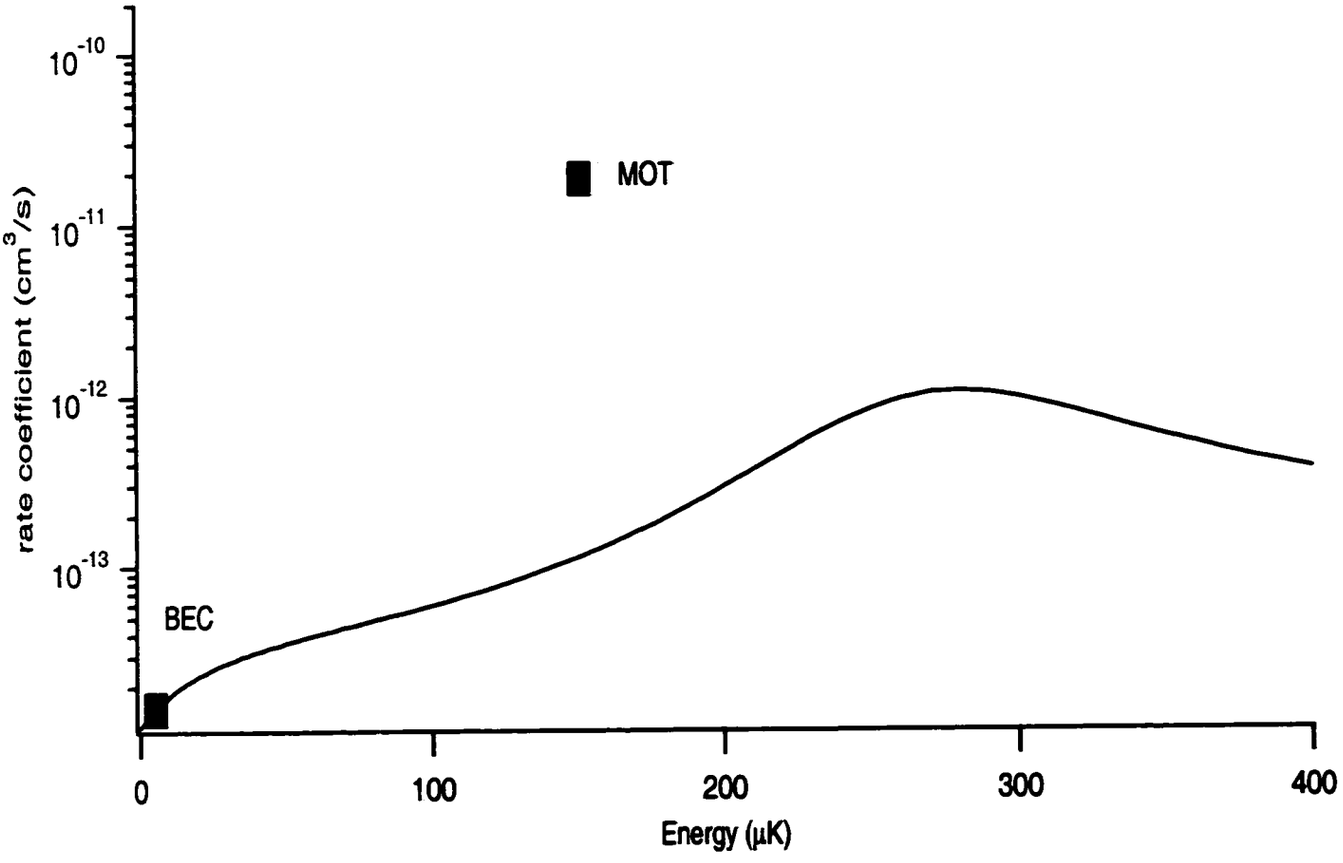

Figure 2.6: Spin-exchange rate as a function of temperature as calculated by [Williams 98]. The loss rate for the MOT of 2×10^{-11} cm^3/s as reported in [Gensemer 97] is shown at a typical MOT temperature of 150 μK. The double BEC result 2.2×10^{-14} cm^3/s [Myatt 97] is similarly shown at the 500 nK.

A second fundamental difference between the two experiments is the presence of light in the MOT case. Bose-Einstein condensation is achieved in a magnetic trap, using a standard MOT only as a starting point. Once the atoms are actually condensed, however, aside from imaging, there is no light present. On the other hand, the measurements in the MOT are made in the presence of the near-resonant trap laser. Thus it seems probable that the presence of the trap laser may affect the spin-exchange process in some way. Intensity dependent measurements have been studied in the previous MOT experiments, and careful examination of the lowest intensity points in figure 2.5 does show a possible decrease for intensities below 2mW/cm^2. If the lowest data point is not considered, the decrease seems quite plausible. The data is plotted on a log scale which tends to hide any possible decrease. At the time of those experiments, there was no basis for believing that the rates should go down at low intensity. In contrast to previous work on this subject, we have measured these rates at much lower trapping intensities.

Chapter 3

Apparatus and Experiment

3.1 Introduction

The discovery of intensity-dependent trap loss in weak magneto-optical traps was made using trap loss measurement techniques in a standard MOT. A general introduction to laser cooling and trapping is given in [Foot 91], and a list of references for various atom trapping experiments is presented in [Newbury 96]. This chapter describes the basic MOT apparatus making particular note of the aspects that are unique for low-intensity traps as well as the techniques used to measure trap loss in low intensity MOT's.

In order to measure ultracold collisions the loss rate due to background collisions must be kept quite small, requiring very low background pressure. Low background pressure is especially important for low-intensity trap loss measurements and is below 10^{-11} Torr in these experiments. A description of the preparation of the ultrahigh vacuum chamber is presented in section 3.2. The optical system, consisting of three external-cavity diode lasers and associated optics and spectrometers, is described in the following section. The vacuum chamber and optical system are pictured in figure 3.1. Trap loss is measured by monitoring the trap density as a function of time. The

fourth section details the various detection methods for determining the density and outlines the equipment used in the detection process. Low intensity traps are much more sensitive to the alignment of the trapping lasers and positioning of the magnetic field zero than ordinary MOT's. The fifth section describes the methods used for trap alignment. Finally, the last section describes the procedure for measuring trap loss rates, including methods for data analysis, important experimental considerations in this regime and sources of systematic errors.

3.2 Vacuum Chamber

Loss of atoms from the trap due to collisions with hot background gas atoms can easily overwhelm the ultracold collision loss especially for weak traps. Thus the quality of the vacuum is extremely important in these experiments. To minimize the background pressure, the vacuum chamber was carefully cleaned following a thorough ultrahigh vacuum cleaning procedure prior to assembly. A detailed set of instructions for this procedure is given in Appendix A as well as the procedure for cleaning copper for use in ultrahigh vacuum environments. After assembling the chamber, we baked it at a temperature of ~220°C over eight days while it was connected to a turbo pump. The heating and cooling were done slowly — over 2-3 days — in order to prevent damage to the windows. Once the chamber reached 220°C we maintained that temperature until the pressure came down by a factor of five.

After initially pumping down the chamber with a turbo-pump, the pressure in the chamber was improved and maintained with two pumps. The first was an 11 L/s Perkin Elmer ion pump. In addition, a Varian mini Ti-ball titanium sublimation pump was used. The combination of careful cleaning and baking as well as high pumping speed resulted in pressures below 10^{-11} Torr. Trap lifetimes as long as 1000 seconds have

Figure 3.1: Picture of the optical table showing the vacuum chamber (left), lasers (right), and the optics required for the experiement.

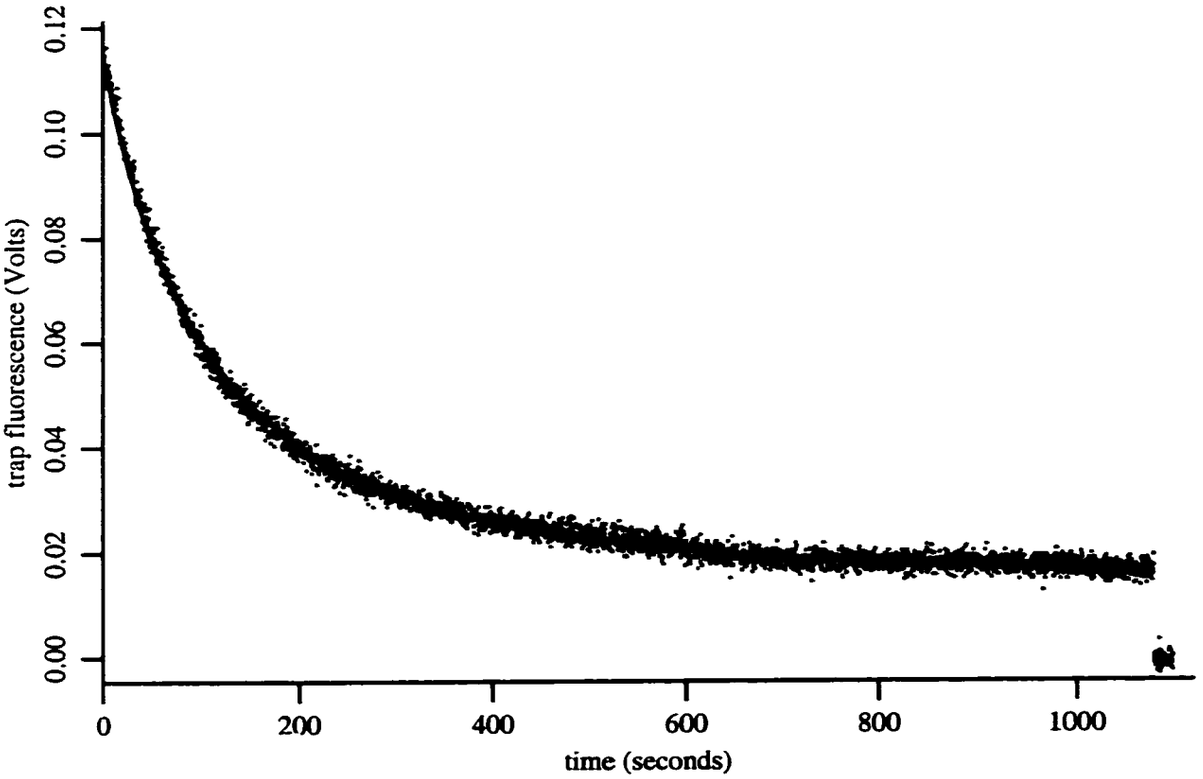

Figure 3.2: Typical trap decay curve showing the extremely long trap lifetime. A fit to the decay gives a background loss rate of .00124s^{-1} corresponding to a trap lifetime of just over 800 seconds. The contribution to ultracold collisions is observed as non-exponential decay. This decay curve was taken at an intensity for which the loss rate due to ultracold collisions is a minimum.

been measured. A typical trap decay curve showing the extremely long trap lifetime is shown in Figure 3.2. A fit to the decay gives a background loss rate of 0.00124s^{-1}, corresponding to a trap lifetime of just over 800 seconds. Longer lifetimes have been observed when the background rubidium pressure was lower.

Rubidium is introduced into the chamber through an atomic beam valve every couple of months. The beam valve consists of a rotary motion feedthrough, with a hole drilled through its shaft, inserted radially into a blank flange. The blank flange has a drilled though its center such that rotation of the feedthrough can align the holes in the feedthrough and flange allowing atoms to stream out of the oven, or misalign the apertures by 90 degrees blocking the flow of atoms. A second aperture was originally

included to collimate the atomic beam. The beam valve was designed to create a beam-loaded trap, allowing the loading to be stopped by rotation of the feedthrough. After many months of use, however, we determined that the source of atoms did not turn off when the beam valve was closed. The chamber wall opposite the beam valve as well as parts of the beam valve itself were presumably coated with rubidium, and thus the trap could be operated for several weeks with the beam valve closed. The trap was therefore not beam loaded, but rather was primarily loaded from a background vapor. Opening the beam valve was simply increasing the background of rubidium vapor available for trapping. After realizing the importance of low rubidium background pressure for our experiments, the beam valve was kept closed during data taking, and extra rubidium was loaded into the chamber by heating the oven behind the valve and then opening the valve for several minutes to an hour only every few months.

An additional feature of the vacuum chamber is the 10″ recessed flange. The recess allows magnetic field coils to be much closer together than otherwise possible. The coils used for this work were wound with three layers of copper tubing for water cooling if necessary. Each coil consists of 102 turns with the inner radius of each coil equal to 4.27 cm and a separation of 6 cm, giving an axial magnetic field gradient of 3.8 G/cm/A.

3.3 Lasers and Optical System

Three lasers were used for this experiment, the trap laser, hyperfine pumping laser, and an additional trapping laser. All three lasers were external cavity, grating-stabilized tunable diode lasers operating at the 780nm $5S_{1/2}$ to $5P_{3/2}$ transition of ^{87}Rb. The external cavity is produced using a diffraction grating in the Littrow configuration to couple the light back into the laser diode. The zeroth order of the grating is used to couple the light out of the laser. The trapping lasers were constructed using the

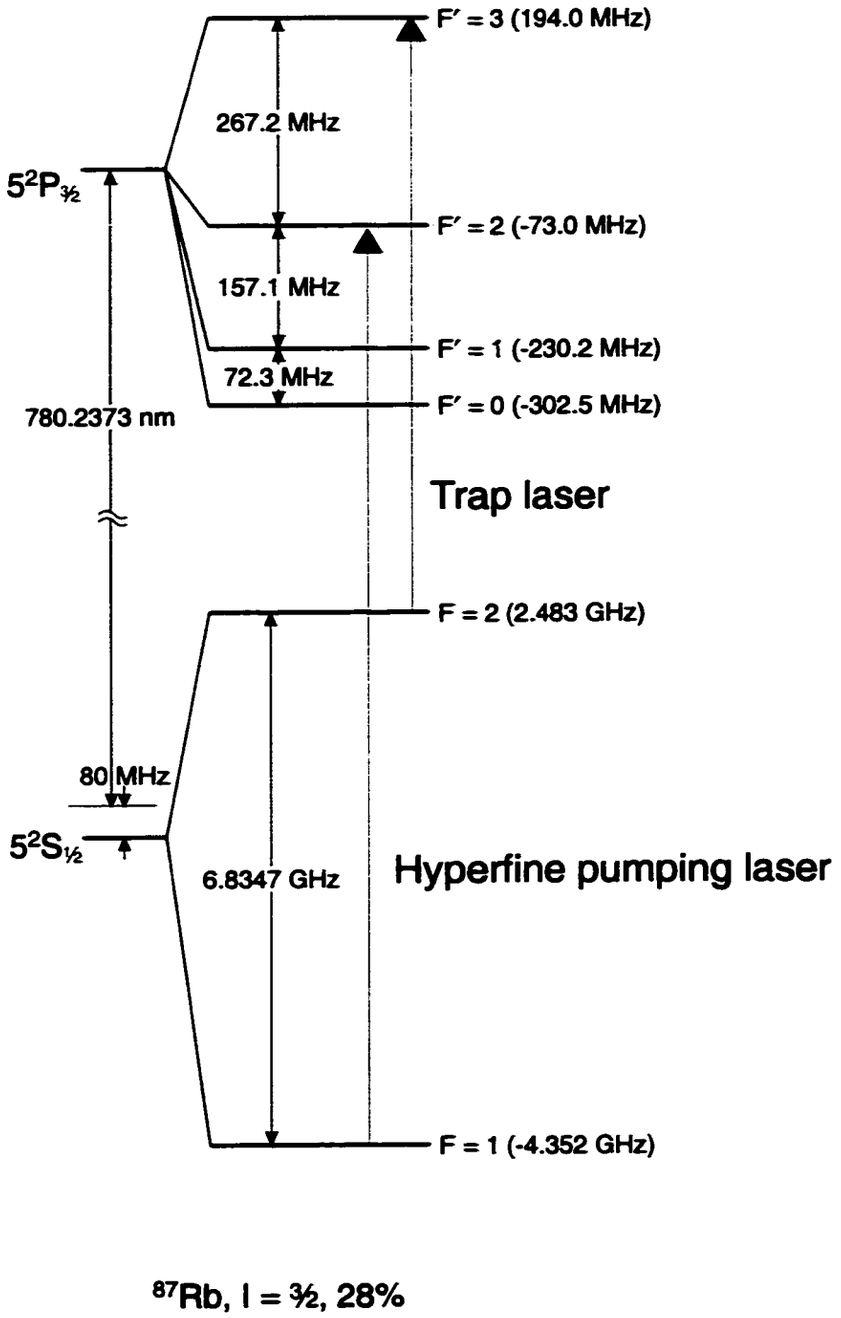

Figure 3.3: Energy level diagram for ^{87}Rb including the frequncies of the trapping and hyperfine pumping lasers

design of [Arnold 98], which involves mounting the laser diode and collimating lens to the stationary portion of a standard mirror mount. The diffraction grating is then attached to an extension of the movable part of the mount. A piezoelectric transducer is inserted in the path of one of the adjustment screws of the mirror mount to allow the position of the grating to be swept, thereby sweeping the frequency of the laser. The hyperfine laser was constructed using a similar design.

An energy level diagram for ^{87}Rb is shown in figure 3.3 with the trap laser and hyperfine pumping transitions noted. All three lasers were locked using saturated absorption spectrometers.[Preston 96] The frequencies of the various transitions in the saturated absorption spectrum as the laser frequency is swept are shown in figure 3.4. A sample saturated absorption spectrum is then shown in figure 3.5. The hyperfine laser was locked on resonance to the F=1 to F′=2 transition. The trap lasers were each offset locked to the F′=2,3 crossover peak using a 140 MHz acousto-optic modulator in the saturated absorption spectrometer. A voltage controlled oscillator was used to set the frequency of the AOM. The crossover peak is 133.6 MHz from the trapping transition, thus by setting the AOM frequency to 127.7 MHz, the trap laser would be set to 5.9 MHz, equal to one natural linewidth, Γ. The primary trap laser detuning was varied between -1Γ and -2Γ, while the additional trap laser detuning was always -1Γ.

A schematic of the essential optical elements is shown in Figure 3.6. The primary trap laser and the hyperfine laser were coupled into a polarization-maintaining fiber using a polarizing beam splitter. Coupling through the same fiber ensured that the two lasers were perfectly spatially aligned. The fiber also eliminated the need for realignment of all of the trapping optics when adjustments were made to either laser. One disadvantage of the polarization-maintaining fiber was the need for extremely precise polarization mode matching. If the polarizations were slightly misaligned, cross-

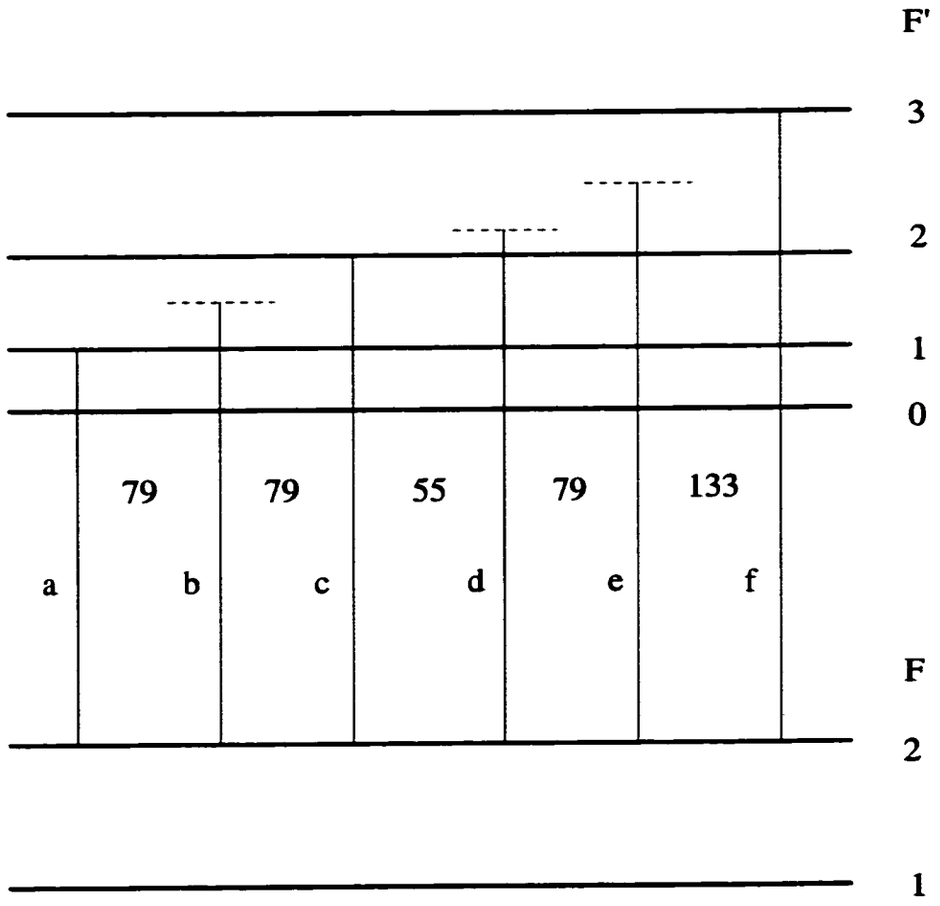

Figure 3.4: Hyperfine levels and F=2 → F′=1,2,3 transitions for ^{87}Rb. The numbers indicate the separation of the various transitions in MHz. The dashed lines indicate the frequencies of cross-overs in the saturated absorption spectrum.

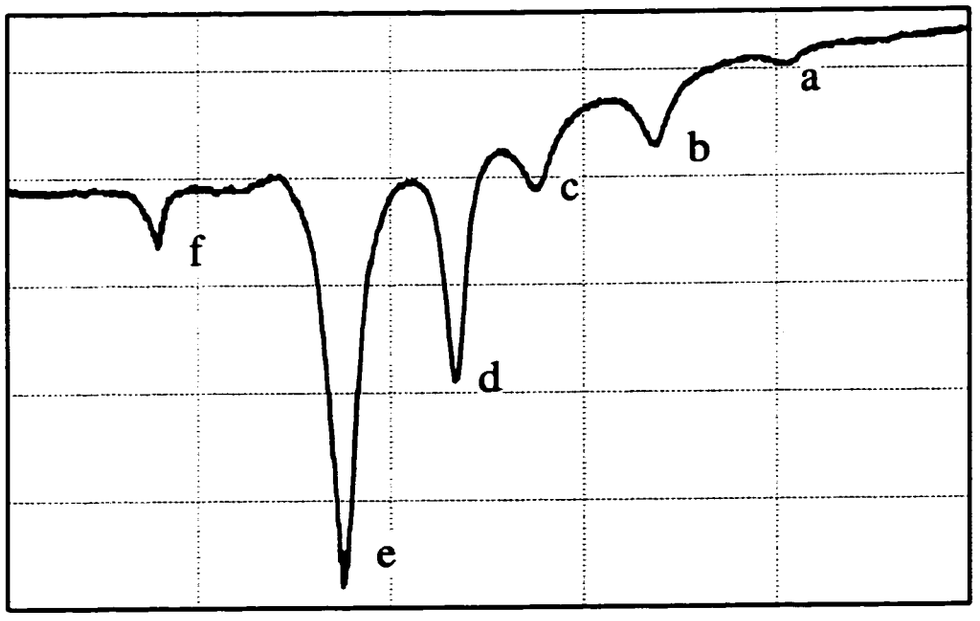

Figure 3.5: Sample saturated absorption spectrum for ^{87}Rb. The letters correspond to the transitions shown in figure 3.4.

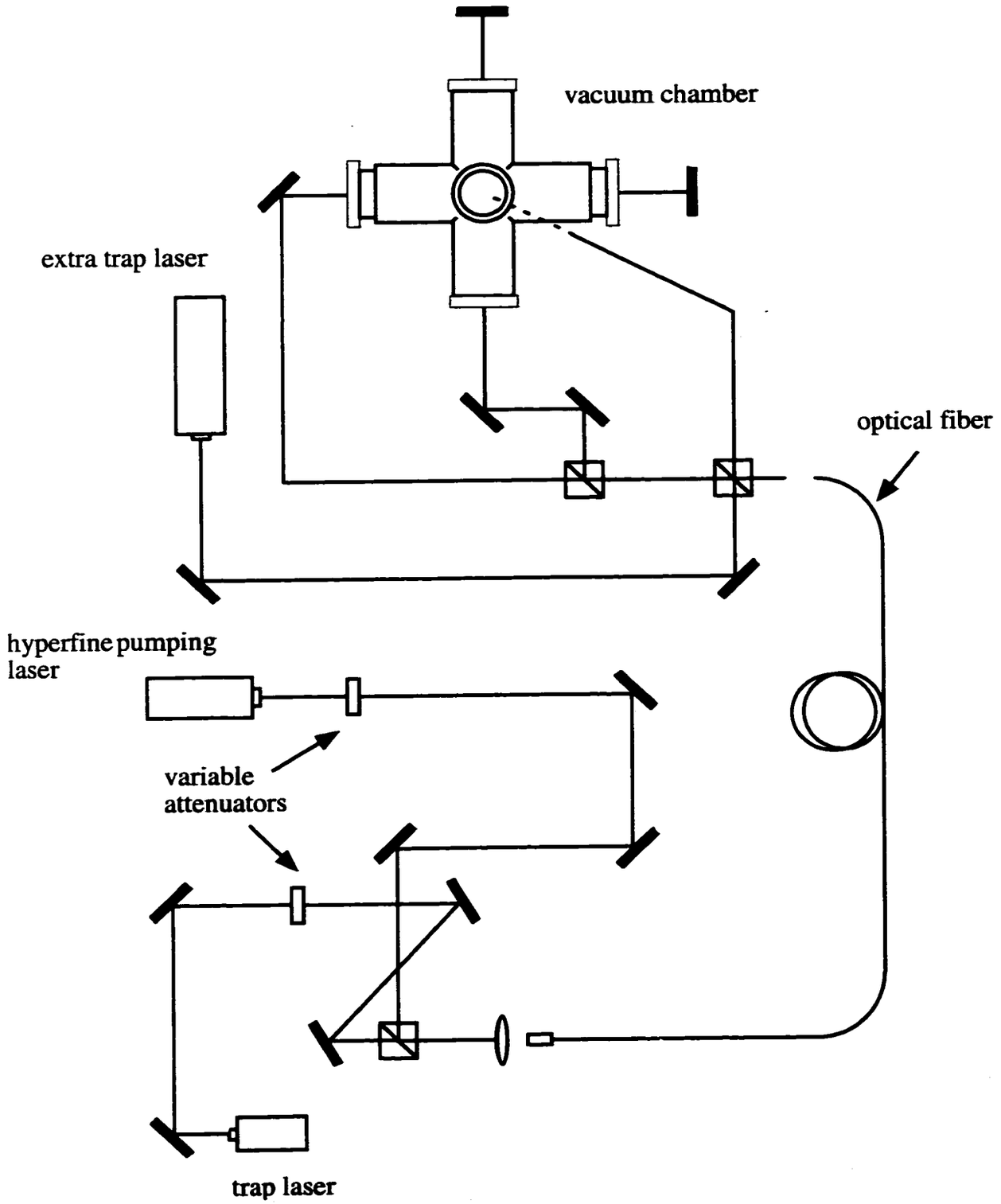

Figure 3.6: Schematic of laser paths and related optical elements.

talk between the polarization modes of the fiber would result in fluctuations of the output polarization. In our experiment that polarization fluctuation translated into fluctuations in the relative trapping beam intensities, dramatically disrupting the trap performance. Careful alignment of the polarizations was achieved by rotating a half-waveplate immediately before the fiber in .1° increments to minimize the intensity fluctuations over several minutes at each waveplate position.

In the paths of the trap and hyperfine pumping lasers was a liquid crystal variable attenuator. The attenuators (Thorlabs, model CR-100) were used as variable waveplates whose retardance was determined by an applied voltage. Because the lasers were coupled into the fiber through a polarizing beamsplitter, rotation of the polarization also changed the amount of light coupled into the fiber, allowing adjustment of both laser intensities. The maximum intensities of the trap and hyperfine pumping lasers were 14 mW/cm^2 and 2 mW/cm^2 respectively.

The polarizations of the each of the trapping beams were set using "Natalie's theorem".[Vansteenkiste, 93] Natalie's theorem provides tests such that the polarization at a retroreflection can be determined by setting the initial polarization and adjusting a quarter-waveplate and half-waveplate while monitoring the return polarization. The benefit to this method is that the circular polarization can be set at the trap independent of any birefringent effects of the mirrors.

The third laser, used as an additional trapping laser, was coupled into the trapping optics through the first beam splitter after the fiber. The diode was a high power Sanyo diode, and provided about 50 mW of power for trapping. This laser was used solely to aid in loading of the trap in order to increase the number of atoms as well as to decrease the time it took to fully load the trap. The laser was blocked using a mechanical shutter during actual data collection.

3.4 Detection

The number of atoms in the trap was measured by imaging the trap fluorescence onto a photodiode. To convert the photocurrent into the number of atoms we first need the scattering rate per atom, R, which is given by

$$R = \frac{\Gamma}{2} \frac{\frac{I}{I_s}}{1 + \frac{I}{I_s} + 4\frac{\Delta^2}{\Gamma}} \tag{3.1}$$

where Δ is the laser detuning from resonance, I is the total laser intensity, I_s is the saturation intensity, and Γ is the natural linewidth. By taking into account the solid angle, Ω, subtended by the imaging system and comparing the number of photons per second scattered from the trap to the scattering rate of a single atom, we can determine the number of atoms in the trap:

$$\text{Number of atoms} = \frac{I_{pd}\eta_e}{\frac{hc}{\lambda} R\Omega} \tag{3.2}$$

where I_{pd} is the photocurrent, η_e is the photodiode efficiency and $\frac{hc}{\lambda}$ is the energy per photon for $\lambda = 780$nm.

For measuring ultracold collisions we need to know how the trap density changes in time, so in addition to the number of trapped atoms we also need to know the spatial extent of the trap. To determine the density the trap was imaged onto a a Princeton Instruments model LN/CCD-512-TKB/4 liquid-nitrogen cooled CCD camera. The program IPLab Spectrum was used to control the camera shuttering as well as to analyze the trap images. The trap density was determined from the two dimensional image by measuring the mean and root-mean-square pixel brightness. From the rate equation (2.1) we can define a reduced volume, the number of atoms divided by the density, as

$$V' = \frac{(\int n d^3r)^2}{\int n^2 d^3r}. \tag{3.3}$$

The modified rate equation including the reduced volume is discussed in section 3.6. Assuming that the density can be written as $n(r) = X(x)Y(y)Z(z)$ then the reduced volume can be written as three separate integrals. Further assuming that the trap is isotropic, so that the density distribution in each direction is equal, the reduced volume can be written as

$$V' = [\frac{(\int X dx)^2}{\int X^2 dx}]^3. \tag{3.4}$$

The numerator is simply the square of the mean of X, and the denominator is the square of the root mean square of X. We can then relate that expression to the two dimensional image in terms of the average and rms pixel brightness by

$$V' = [\frac{(\int n dx dy)^2 K_{pixel}^2}{\int n^2 dx dy}]^{3/2} = [\frac{N^2 \overline{n}^2 K_{pixel}^2}{N n_{rms}^2}]^{3/2} \tag{3.5}$$

where N is the total number of pixels and K_{pixel} is the conversion factor between pixels and centimeters. Up to two additional inexpensive CCD security television cameras were used to monitor the trap for diagnostic purposes.

Finally, the timing of the entire experiment is controlled using a National Instruments data acquisition (NIDAQ) board with a Power Macintosh 7100. The NIDAQ board controls the voltages for setting the variable attenuators, changing the magnetic field gradient, opening and closing the shutter, and taking images of the trap. In addition, the trap fluorescence data from the photodiode were collected and stored with the NIDAQ board.

3.5 Trap Alignment

Over the course of developing the experiment, it became clear that the alignment of the trap was critical to the operation of very low intensity traps, especially below 1 mW/cm^2. The two indications used for setting the alignment were the slow, uniform

dissipation of the optical molasses as the magnetic field gradient was turned off and the spatial stability of the trap as the laser intensity was modulated. After using those two as diagnostics for aligning the trap, the minimum intensity feasible for operating the trap was measured by modulating the trap intensity between the maximum and minimum and requiring the number of trapped atoms remained constant.

Optical molasses describes the atoms in the six trapping beams in the absence of a magnetic field gradient.[Chu 85] In this configuration the atoms undergo a random walk and eventually leave the intersection region of the trapping beams. If the trapped atoms begin in the center of the intersection region and the intensities of the six beams are well balanced, the optical molasses will dissipate slowly and uniformly. If, on the other hand the atoms start on the edge of the intersection region, the force on the atoms will not be balanced and the cloud of atoms will expand much more quickly in one direction than the others. Thus if the zero of the magnetic field gradient is well centered in the intersection of the six beams, when the gradient is turned off, the molasses will be slow and uniform. To monitor the molasses in three dimensions, two CCD cameras were used looking along two different axes of the trap, while the magnetic field was switched on and off. The duty cycle was adjusted to maximze the number of atoms loaded into the trap thus maximizing the fluorescence. In addition to the standard anti-Helmholtz coils there were three sets of shim coils used to cancel the effects of stray field. These shim coils were used to center the zero of the field on the beams.

The spatial stability of the trap was also monitored with the two CCD cameras. In this case the trap intensity was modulated between the maximum intensity (10-15 mW/cm^2) and some lower value. The retroreflecting mirrors were adjusted so that the trap position did not change as the intensity changed. The low intensity value was decreased as the alignment approached an equilibrium to make the procedure

as sensitive as possible. The retroreflection positions were further restricted by the requirement that any intereference lines in the trap be eliminated.

These two alignment procedures were complicated by the fact that the two adjustments were coupled. Thus the alignment was an iterative process. In addition, the separate procedures were not easy as each involved three different axes of adjustment. Once the two procedures seemed to converge, the trap operation at low intensity was checked by switching the trap intensity from the maximum value down to very low values – below 1 mW/cm^2 for 0.5 sec. and then switching the intensity back to the original value. For a well-aligned trap, the number of atoms should remain constant during this process. The low intensity was decreased until the number of atoms showed a decrease, thus determining the lowest intensity used for taking loss rate measurements. This check also served as a diagnostic for ensuring that the two alignment procedures had converged. We have also used a slight variation of this diagnostic as a method for measuring the excited state fraction in the trap. Details of this new technique are described in chapter 6.

3.6 Experiment

We are interested in measuring the loss rate due to ultracold collisions as a function of the trap laser intensity. To perform the basic experiment the trap was loaded with both trap lasers at their maximum intensities. The trap was loaded for 15 seconds to 2 minutes, depending on experimental parameters such as laser detuning. The loading time is related to the trap density which is discussed following the outline of the experimental procedure. Once the trap was sufficiently loaded, the trap laser intensity was switched to a lower value using a variable attenuator as described in section 3.3. The atoms were then allowed to decay from the trap for up to 15 minutes.

During the loading and decay processes the fluorescence signal from the trapped atoms was recorded. An image of the trap was taken with the liquid-nitrogen cooled CCD camera 5 seconds after the intensity was changed for measuring the density. We were operating the trap in a low-density regime, for which the volume of the trap does not change as the number of atoms changes. A second image was taken at the end of the decay with the magnetic field gradient turned off to allow for background subtraction. A typical data set is shown in Figure 3.7.

To determine the ultracold collision loss rate, the decay portion of the data was fit to the solution of the rate equation

$$\begin{aligned} \frac{dN}{dt} &= L - \Gamma N - \beta \int n^2 d^3r \\ &= L - \Gamma N - \beta N \frac{\int n^2 d^3r}{\int n d^3r} \end{aligned} \tag{3.6}$$

where N is the number of trapped atoms, n is their density in atoms/cm^3, L is the loading rate in atoms/s, Γ is the loss rate due to collisions with background gas in s^{-1}, and β is the ultracold collision loss rate coefficient in cm^3/s. Using the reduced volume, V$'$, defined in equation 3.3, the loading equation then becomes

$$\frac{dN}{dt} = L - \Gamma N - \frac{\beta}{V'} N^2 \tag{3.7}$$

whose solution can be written as:

$$N = N_{off} + N_o + \left[\left(\frac{1}{N_o - N_\infty} + \frac{\beta/V'}{\Gamma + 2N_\infty \beta/V'} \right) e^{(\Gamma + 2N_\infty \beta/V')t} - \frac{\beta/V'}{\Gamma + 2N_\infty \beta/V'} \right]^{-1} \tag{3.8}$$

where N_{off} accounts for the offset in the fluorescence signal due to scattered light and N_o is the initial number of atoms. N_∞ represents the equilibrium number of atoms and includes the effects of loading. The relationship between N_∞ and the loading rate, L,

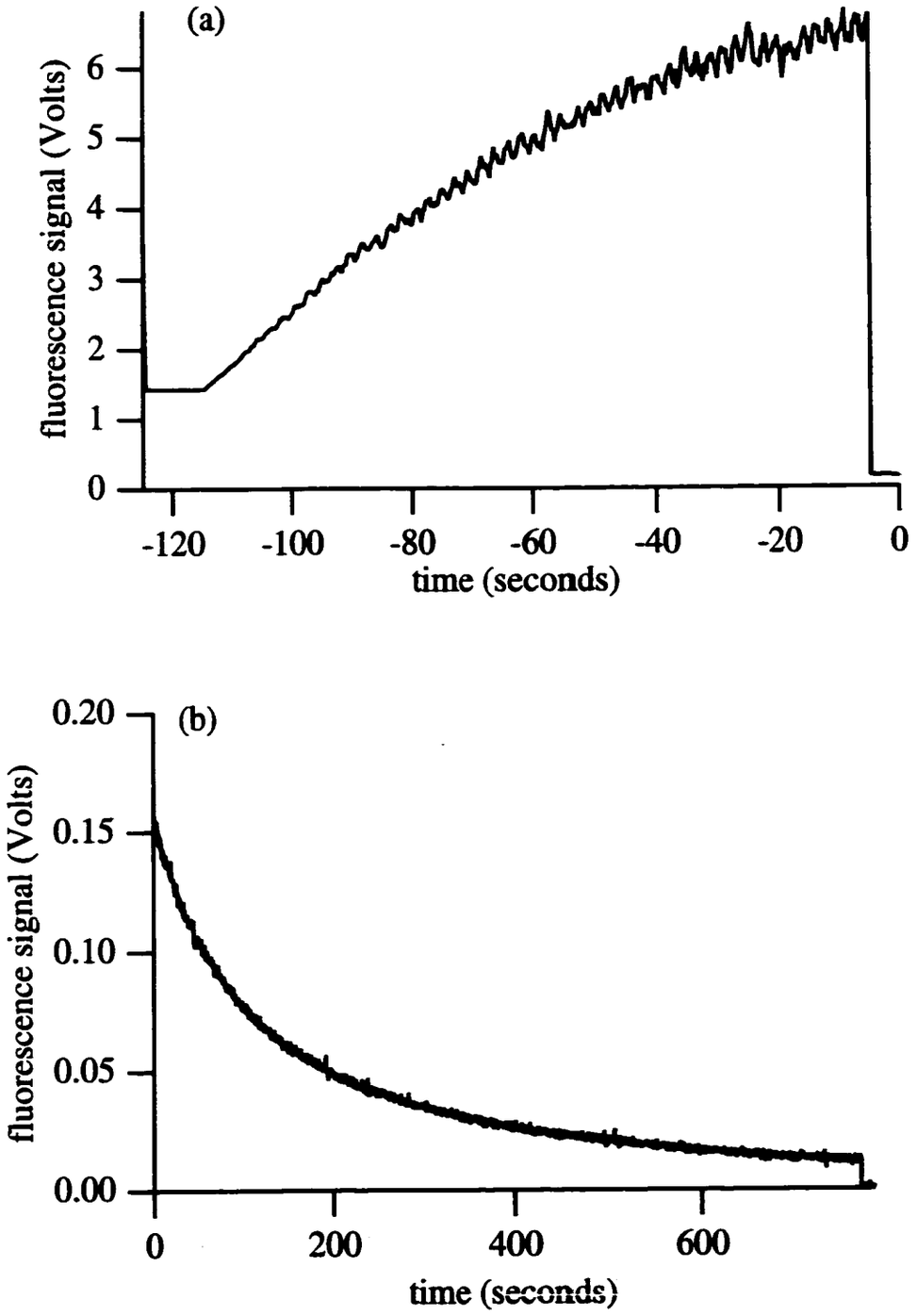

Figure 3.7: Sample data for measuring β. (a) The trap was loaded for 2 minutes at high intensity. (b) In this case the intensity was then decreased to 0.5 mW/cm^2 and was then allowed to decay for 13 minutes. β is determined by fitting the data in (b) to the analytic solution of the trap loading rate equation.

is given by

$$L = \Gamma N_\infty + \frac{\beta N_\infty^2}{V'} \tag{3.9}$$

Without loading, N_∞ would be equal to zero.

To further account for loading in our experiments a loading transient was measured at each intensity. The loading curves were taken by setting the trap intensity to the value of interest. The magnetic field gradient was set to zero for 10-20 seconds in order to account for scattered light and then was set back to 10-20 G/cm. The trap was then allowed to load atoms at the reduced intensity for 15 minutes. The loading curves are similar to the one shown in figure 3.7. As in the decay curves, the fluorescence was monitored during the loading, however no CCD image was taken. Each loading curve was then fit to Equation 3.8 to get an estimate of N_∞. The fit also gave values for Γ and β/V', however, the signal to noise, especially at very low intensities, was particularly poor. The value for N_∞ obtained was then used as the starting point in fitting the corresponding decay data. Many low intensity points did not show any loading after 15 minutes. For those points N_∞ was started with a value of zero.

Before fitting the decay, the data were first filtered with a time constant of 1 second to reduce noise. The data were then fit to equation 3.8 using a least squares fit in the commercial data analysis program IGOR. The filtering and fitting functions for IGOR are given in Appendix B. A sample of the filtered data and the corresponding fit is shown in figure 3.8.

The offset and initial numbers of atoms were fixed during the fit, while the remaining three fitting parameters,Γ, β/V', and N_∞, were variable. The long decay time allowed for a more accurate determination of the contribution from background collisions. On the some of the lowest intensity points, the fit resulted in a negative value for N_∞ that was not within statistical error of zero. In those cases, the final number of atoms was fixed at zero. The reduced volume, V', was obtained by analyzing the trap image as

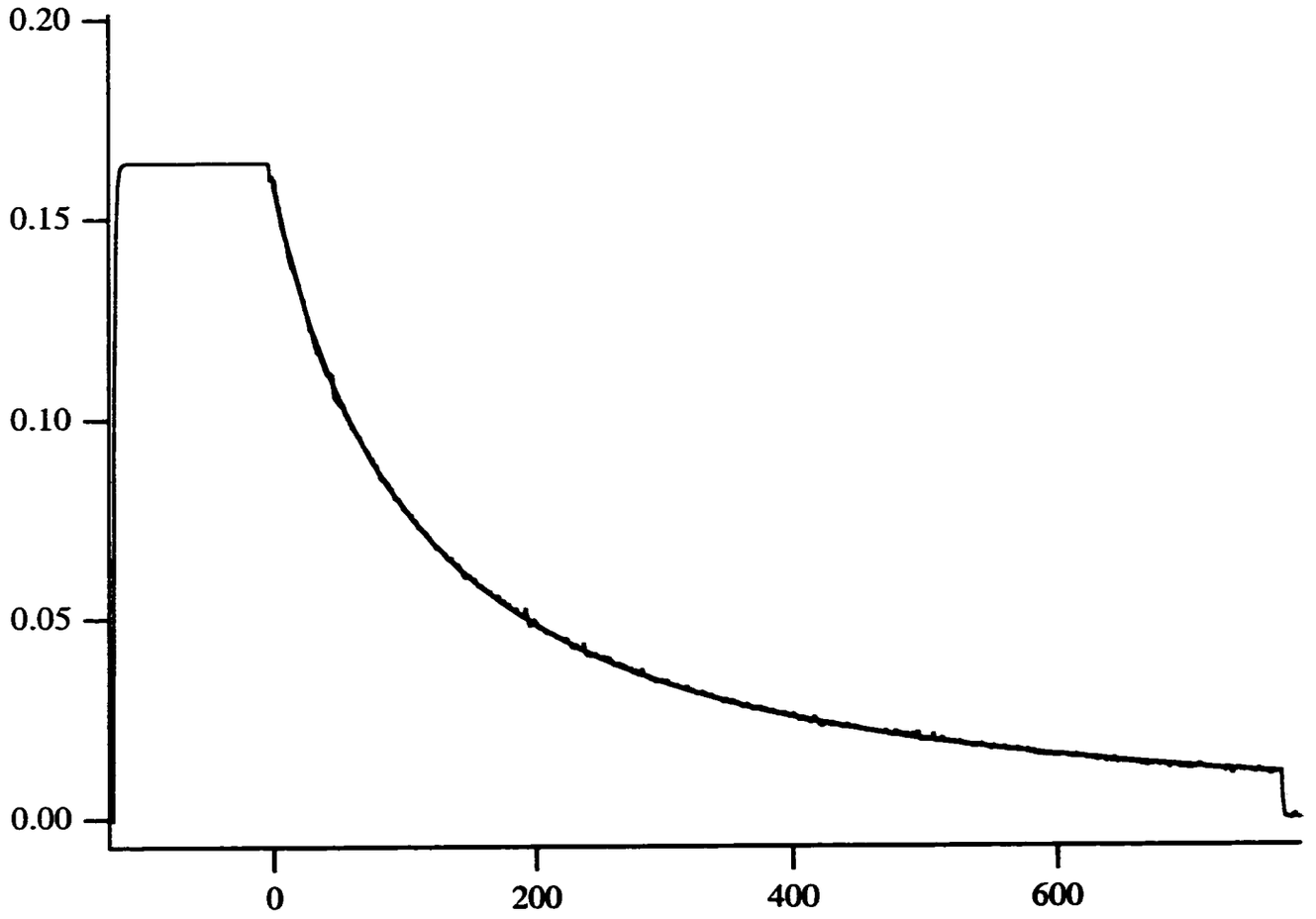

Figure 3.8: Same data as in Fig. 3.7 after filtering and the fit to the data.

described in section 3.4. Combining that volume with the results of the fit gave a value for β.

One of the primary figures of merit for the experiment was the parameter $\frac{2\beta N_o}{\Gamma V'}$. This parameter gives an indication of the relative importance of ultracold collisions compared to background collisions for a given density. In order for the ultracold loss rate to be clearly distinguishable from the background loss, this parameter must be larger than 1, however it is preferable for the parameter to be on the order of 10 or more. The only experimental control of the figure of merit is the initial trap density. To improve the figure of merit, we wanted to load as many atoms as possible before changing the intensity. Installation of the additional, high-power trap laser provided nearly an order of magnitude increase in the initial number of atoms over our first attempts, dramatically improving the signal to noise.

In these experiments the typical number of trapped atoms was on the order of 10^5 atoms. This number is much smaller than in a typical MOT. The primary limitation to the number of trapped atoms was the very low background pressure. In order to keep the loss rate due to background atom collisions low, the background rubidium vapor-pressure was necessarily kept quite low. Since the trap was loaded from the low-velocity background rubidium atoms in the chamber, the low background resulted in fewer trapped atoms. Thus, we improved our loss rate due to background collisions at the expense of the trap loading.

In contrast to the need for large initial numbers of atoms, there is also a limitation on the initial number. For large numbers of atoms the density can become quite high especially at larger detunings for which the trap volume is small. As a result, the density can easily reach a few times 10^9 atoms/cm^3 or more. As the density increases, the distribution of atoms in the trap changes from the low density Gaussian distribution to a hard sphere distribution. The hard sphere distribution is created by

radiation trapping among the trapped atoms.[Walker 90] Radiation trapping provides a repulsive force between the atoms when a photon emitted from one atom is absorbed by another atom in the trap. Under these conditions the volume of the trap does not remain constant as the number of atoms changes – a critical assumption in our measurements. Thus although large numbers of atoms are important to the figure of merit, care must be taken to keep the density below 10^9 atoms/cm^3. In order to maintain reasonable densities, the loading time was adjusted for each intensity.

The possibility of radiation trapping causing the size of the trap to change as the number of atoms changes is a potential source of error. Care has been taken to keep the density low enough to prevent radiation trapping. Another source of error that is probably the most significant is the trap imaging and subsequent calculation of the reduced volume. The depth of field on the CCD camera was quite small, and thus small movements in the trap position could change the image properties. Furthermore, if the spatial extent of the trap is larger than the depth of field, the image will be smeared out, increasing the measured reduced volume. This effect is most important for weak, low-intensity traps. We estimate that the measured reduced volume could be as much as a factor of 2 larger than the actual volume. The fit parameter for the ultracold collision loss rate is multiplied by the reduced volume in order to obtain the actual loss rate. If the measured reduced volume is too large, the error will make the intensity-dependence less significant rather than creating a false intensity dependence.

Another source of error is the laser stability. When locked the laser frequency noise was as large as 1 MHz, creating a variation in the trap laser detuning. Because a single data point required laser stability over 15 minutes, the stability of the laser was important. For large laser fluctuations the decay of the trap fluorescence was noticeably affected. Data for which serious fluctuations appeared to have occurred was not used. Data taken at larger detunings was most dramatically affected by laser noise. For 2

linewidths detuning, the detuning which suffered most from this noise, data was taken several times at one intensity. The variation in β was no larger than a factor of 2.5. The trap laser was particularly noisy at that time in addition to the trap being more sensitive to the fluctuations. For the majority of the data I estimate that frequency noise introduced a much smaller error, on the order of $\sim$50 percent.

The depth of field issue with the imaging and the reproducibility due to frequency noise are the two largest sources of error. Between these two contributions the accuracy of the data is estimated to be within a factor of 2. Additional sources of systematic errors are polarization fluctuations caused by the optical fiber, which varied by 3 percent and errors in determining the fixed offset parameter in the fit, allowing a potential error of a few percent. Statistical errors in the fit parameters are quite small, and are on the order of 5-10 percent. The overall confidence in the measured loss rates is thus approximately a factor of 2.

Chapter 4

Low Intensity Collision Experiment Results

4.1 Overview

The basic method for measuring the trap loss rates and analyzing the acquired data were described in Chapter 3. In this section the results of the ultracold collision loss rates as a function of trap intensity are presented for a variety of trap parameters. Trap loss rates were measured for three different trap laser detunings: $-\Gamma$, -1.5Γ, and -2Γ. For a laser detuning of $\Delta = -\Gamma$ two magnetic field gradients were examined. Finally, the dependence of the trap loss rate on the intensity of the hyperfine pumping laser was also measured.

4.2 $\Delta = -1\Gamma$

The original experiment was to look at the intensity dependence of the ultracold collision loss rate with a laser detuning of $\Delta = -1\Gamma$. One linewidth detuning is a standard

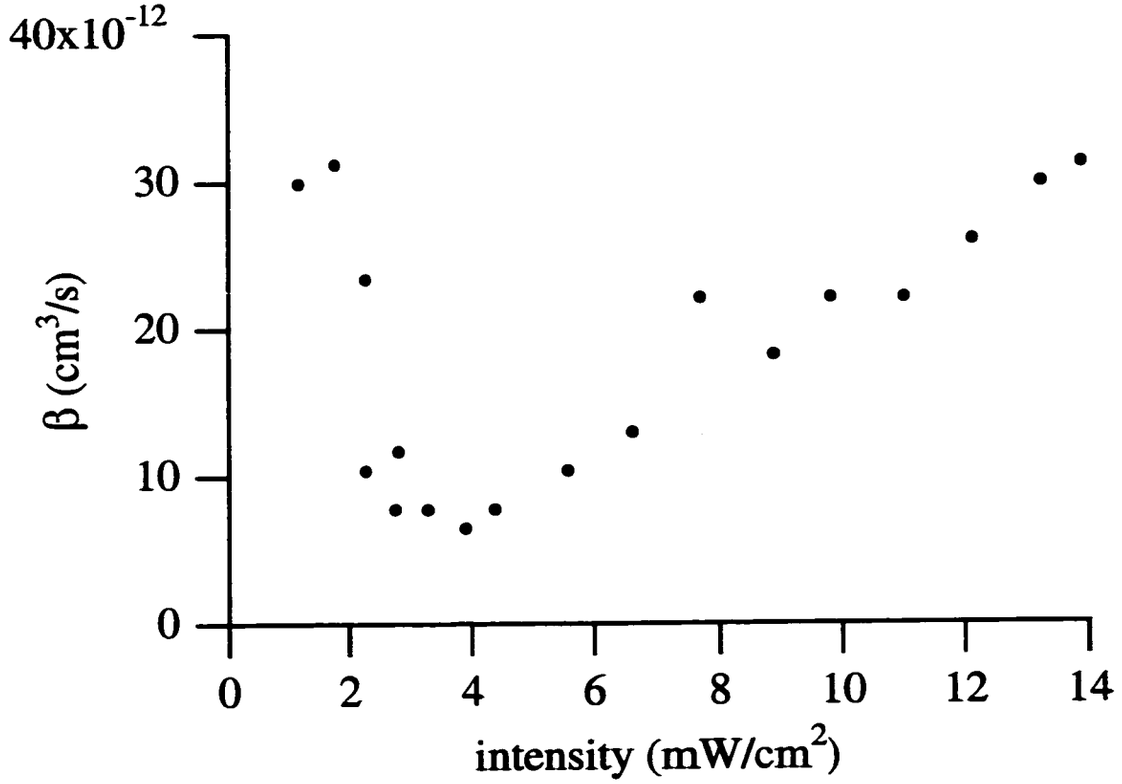

Figure 4.1: Loss rate as a function of intensity for $\Delta = -1\Gamma$ and the magnetic field gradient set at 10 G/cm over entire range of intensities. The rate shows the same behavior as was previously measured by [Gensemer 97]

detuning for MOT's, and the number of atoms that could be loaded into the trap was a maxmimum at this detuning. Initially the magnetic field gradient was set to 10 G/cm. The ultracold collision loss rate, β, was measured over a wide range of intensities to ensure that we observed a similar dependence of β on intensity as was reported by the Connecticut group.[Gensemer 97]. This data shows a factor of two smaller loss rate at high intensities as compared with the Connecticut data. The accuracy of our data is approximately a factor of two, and refinements to the experiment were made after these measurements were taken, thus the difference in high intensity loss rates is not a concern.

After confirming a rapid increase in the loss rate below 4 mW/cm^2 as shown in figure 4.1, attention was focused on intensities below that point. This data compares quite well with the data from the Connecticut group, shown in figure 2.5. The minimum in the trap loss rate occurs at approximately 4 mW/cm^2. Furthermore, the maximum low intensity rate of 3×10^{-11} cm^3/s is comparable to their value of 2×10^{-11} cm^3/s. The low intensity data is shown in figure 4.2. The loss rate increases with decreasing intensity until about 0.8 mW/cm^2. Below that point the loss rate clearly decreases with decreasing intensity.

The trap could effectively trap atoms below the intensity 0.3 mW/cm^2 for which the data ends. Below that point, however, the size of the trap became an issue. As the trap intensity is decreased, the effective volume of the trap increases as the trap becomes weaker. The reduced volume is plotted as a function of intensity in figure 4.3. Recall that the figure of merit for these measurements is $\frac{2\beta N_o}{\Gamma V'}$ where β is the ultracold collision rate coefficient, N_o is the initial number of trapped atoms, Γ is the loss rate due to collisions with background atoms, and V$'$ is the reduced volume. The figure of merit provides an indication of whether the ultracold collision contribution is larger than the background collision contribution. At low intensities the figure of merit suffers

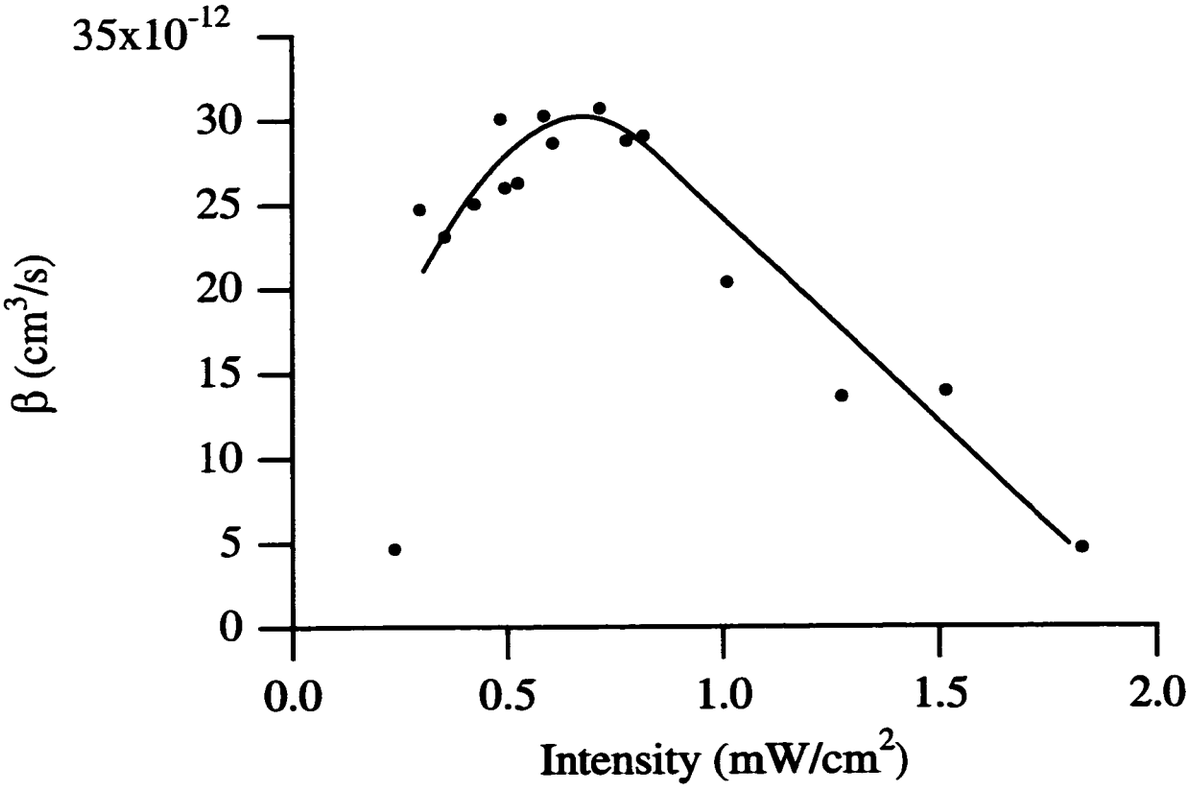

Figure 4.2: Loss rate as a function of intensity at low intensity for $\Delta = -1\Gamma$ and the magnetic field gradient set at 10 G/cm. As the intensity is decreased the loss rate reaches a maximum and then decreases. The intensity dependence at low intensities was previously unexpected. The solid line is there to guide the eye.

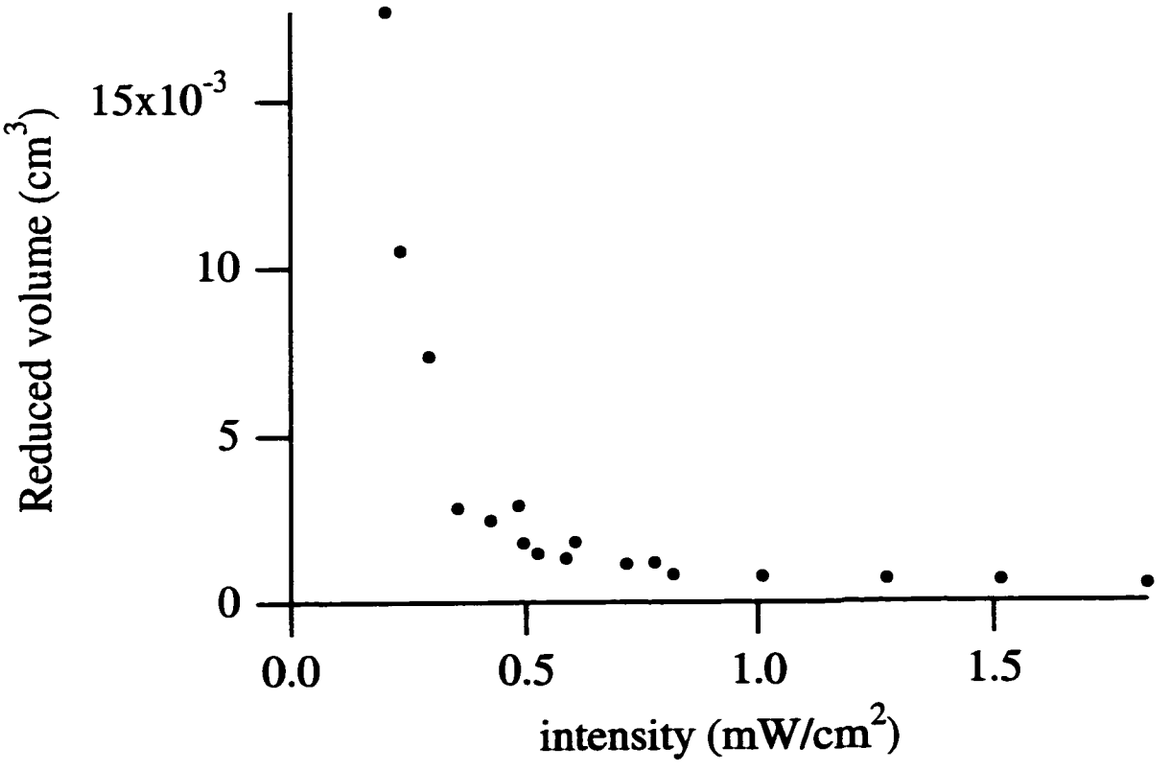

Figure 4.3: Reduced volume as a function of intensity for $\Delta = -1\Gamma$ and the magnetic field gradient set at 10 G/cm. At low intensities the volume becomes prohibitively large, such that the initial density is too low to distinguish the contribution of ultracold collisions from background collisions.

due to the increase in volume.

In order to extend the data reliably to lower intensity it is necessary to start with higher initial densities. Increasing the magnetic field gradient decreases the trap volume, thus the trap loss rates were investigated with a higher magnetic field gradient. The data shown in Figure 4.4 were taken at $\Delta = -1\Gamma$ with the magnetic field gradient increased to 18 G/cm as the trap laser intensity was turned down. The loss transients for data near the peak and and at an intensity below the peak are shown in figure 4.5. In addition to reaching lower intensities, the peak loss rate is higher and occurs at higher intensity. Changing the magnetic field gradient not only affects the density but also alters the trap depth.

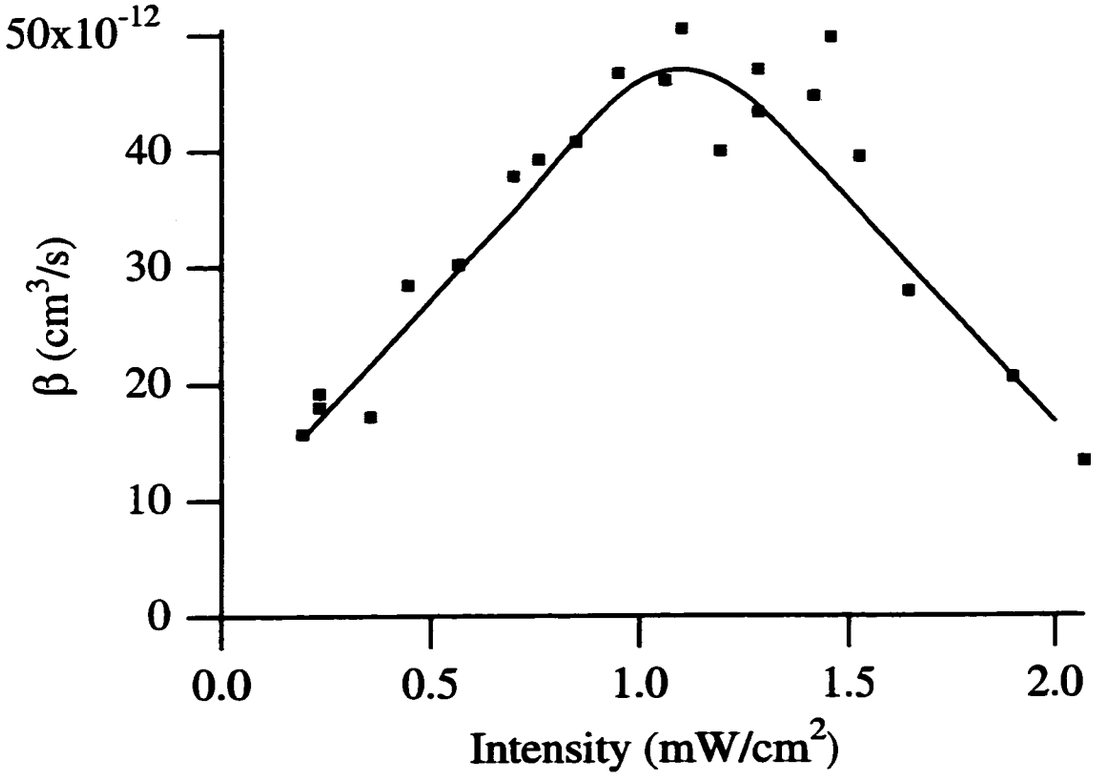

Figure 4.4: Loss rate as a function of intensity for $\Delta = -1\Gamma$ and the magnetic field gradient at 20 G/cm. The shape is similar to the 10 G/cm data, however the peak loss rate is larger and the position of the peak has shifted to higher intensity. The solid line is there to guide the eye.

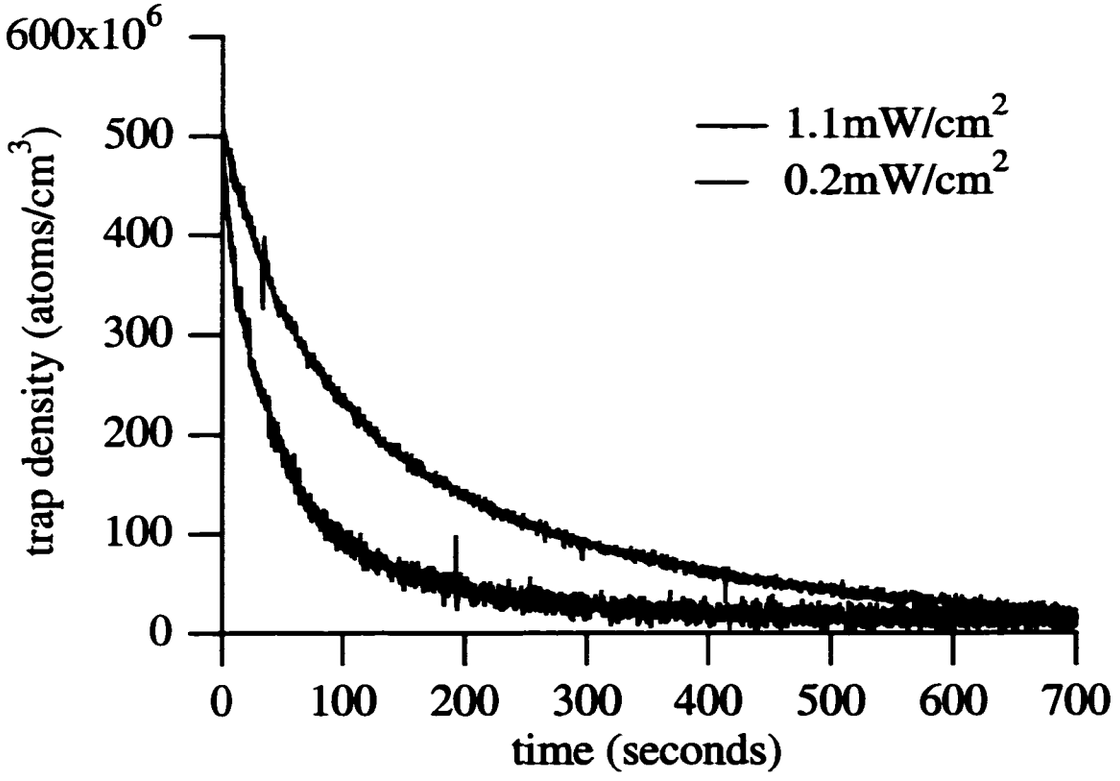

Figure 4.5: Decay transients for .2 and 1.1 mW/cm^2 with the magnetic field gradient at 18 G/cm. The time scale has been shifted to match the inital trap density between the two curves. The loss rate for .2 mW/cm^2 is 1.6 $\times$ 10^{-11} cm^3/s and is 5 $\times$ 10^{-11} cm^3/s for 1.1 mW/cm^2.

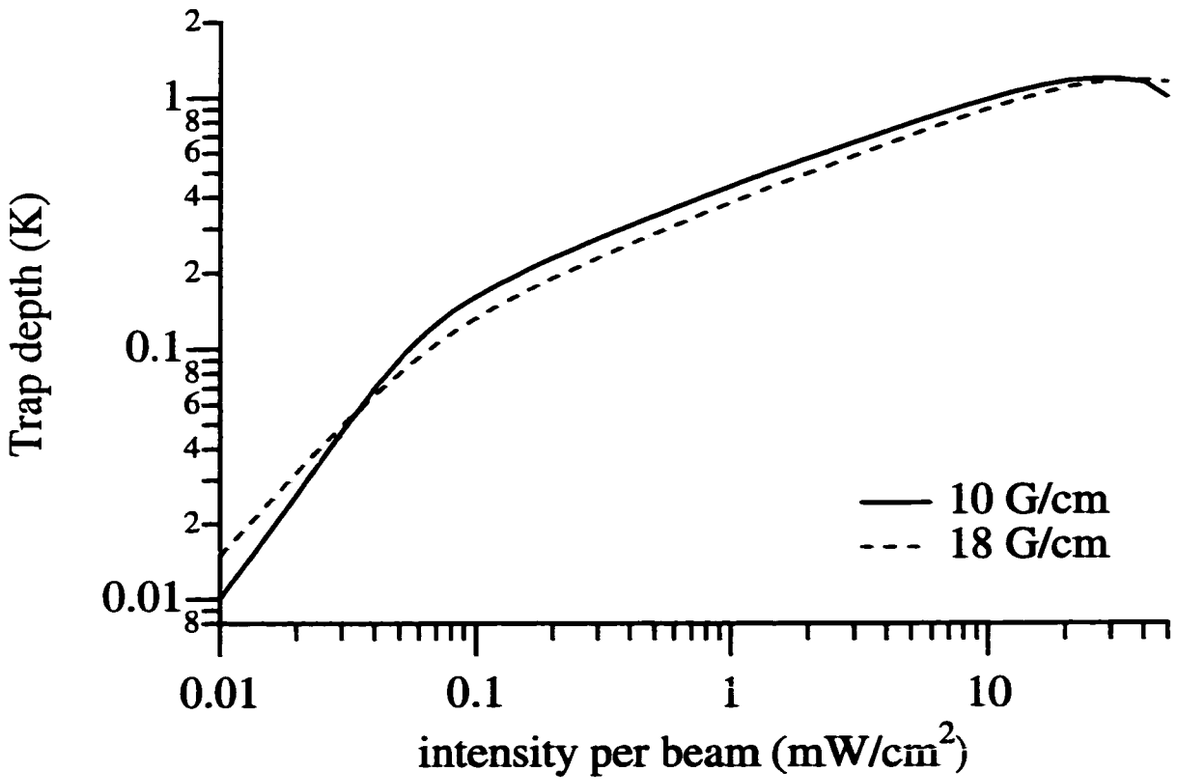

Figure 4.6: One-dimensional trap depth calculations for 10 and 18 G/cm using the algorithm developed by [Gensemer 97]. The trap depth calculations show that at 18 G/cm the trap depth is smaller than at 10 G/cm. The intensity for which the trap loss rate is a minimum depends on the trap depth.

The Connecticut group has developed a computer model to calculate the trap depth in one-dimension for arbitrary trap intensity, trap laser detuning and magnetic field gradient.[Gensemer 97] A comparison of the trap depths using this code for 10 G/cm and 18 G/cm is found in figure 4.6, showing that the trap depth is smaller for the 18 G/cm trap for our intensity range. That means that the point at which the trap cannot recapture atoms that have gained energy equal to the hyperfine splitting will move to higher intensity as the magnetic field gradient is increased. These one-dimensional trap depth calculations serve to give an idea of the dependence on magnetic field gradient, however they are not meant to give absolute value for the trap depth.

The two sets of data at different magnetic field gradients are overlayed in Figure 4.7.

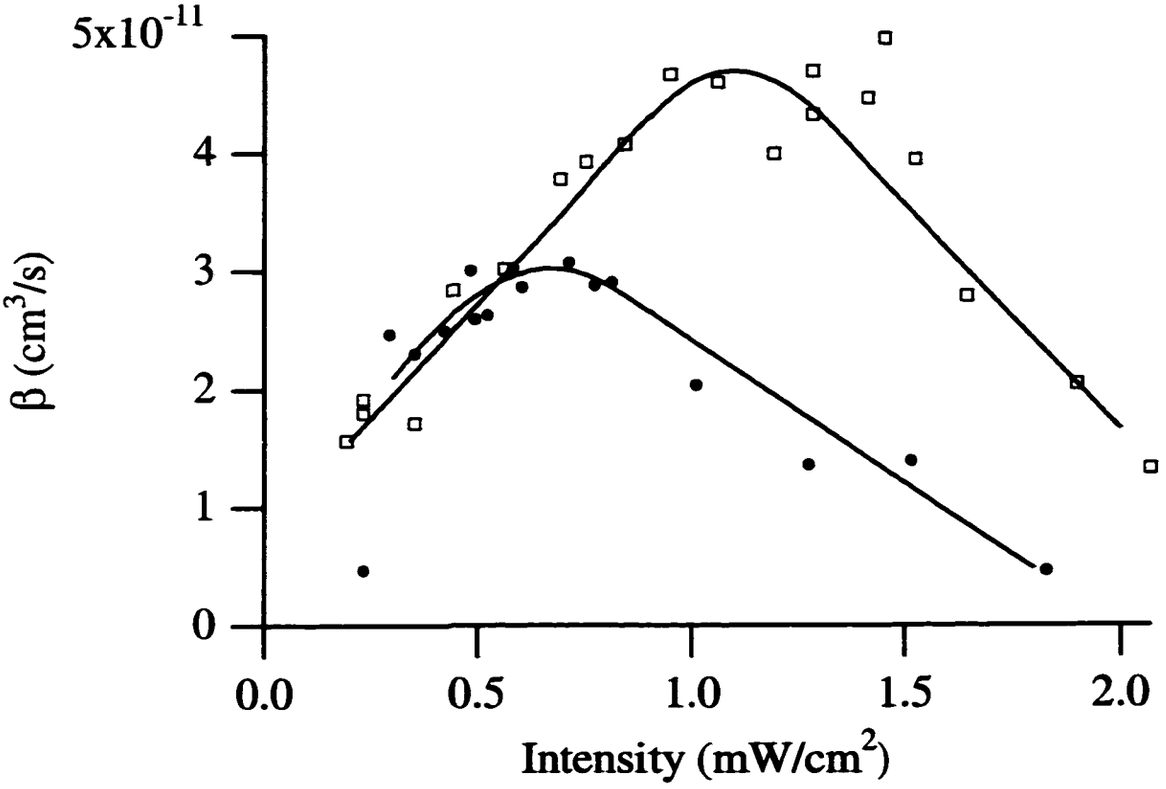

Figure 4.7: Loss rate as a function of intensity for $\Delta = -1\Gamma$ for both magnetic field gradients. The cirles indicate 10 G/cm data, and the squares indicate 18 G/cm data. The low intensity for which the trap loss rate begins to increase is clearly shifted to higher intensities for the larger magnetic field gradient. The solid lines are to guide the eye.

At low intensities, the trap loss rates for the two gradients lie on top of each other. The slopes at low intensity are 3.3×10^{-11} cm^3/s/mW/cm^2 and 3.6×10^{-11} cm^3/s/mW/cm^2 for the 10 G/cm data and 18 G/cm data respectively. It isinteresting that the data taken with the higher gradient continues to increase for larger intensities than the lower gradient data. The intensity for which the loss rate increases has also shifted to larger intensities for the higher magnetic field gradient.

4.3 Higher Detunings

In addition to the one linewidth detuning, loss rates were also measured at $\Delta = -1.5\Gamma$ and -2.0Γ. As in the $\Delta = -1\Gamma$ data, the loss rate is seen to decrease at low intensities rather than reaching a plateau. The data at those detunings is shown in Figure 4.8.

The trap volumes are an order of magnitude smaller at these detunings as compared with -1Γ volumes. The smaller volumes would seem beneficial for improving the figure of merit, however the high densities mean that radiation trapping is a larger concern. It was primarily for these detunings that very short loading times, as short as 15 seconds, were used to limit the initial density. Because the fluorescence signal is smaller for larger detunings, starting with a smaller number of atoms dramatically affected the raw voltages from the fluorescence. As a result the effect of laser noise was a much larger problem in the higher detuning data. The data at -2Γ was most seriously affected by poor signal to noise.

Although the data is noisier than for $\Delta = -1\Gamma$, it should be noted that the peaks for both -1.5Γ and -2Γ detunings shift out to higher intensities. At these large detunings, trap operation was not reliable at intensities much below 1 mW/cm^2 and 2 mW/cm^2 for -1.5Γ and -2Γ respectively. Decreasing the magnetic field gradient in order to alleviate the density problems would not have provided additional information because the peak would shift to lower intensities, already nearly inaccessible. The slope of the low intensity portion of the data is more shallow for the higher detunings than for the $\Delta = -1\Gamma$. For $\Delta = -1.5\Gamma$ the slope is 1.6×10^{-11} cm^3/s/mW/cm^2, and for $\Delta = -2\Gamma$ the slope is approximately 1.4×10^{-11} cm^3/s/mW/cm^2. Especially in the -2Γ case, the poor signal to noise creates large uncertainty in the slope. It is clear, however, that the slope of the loss rate as a function of intensity depends on the detuning.

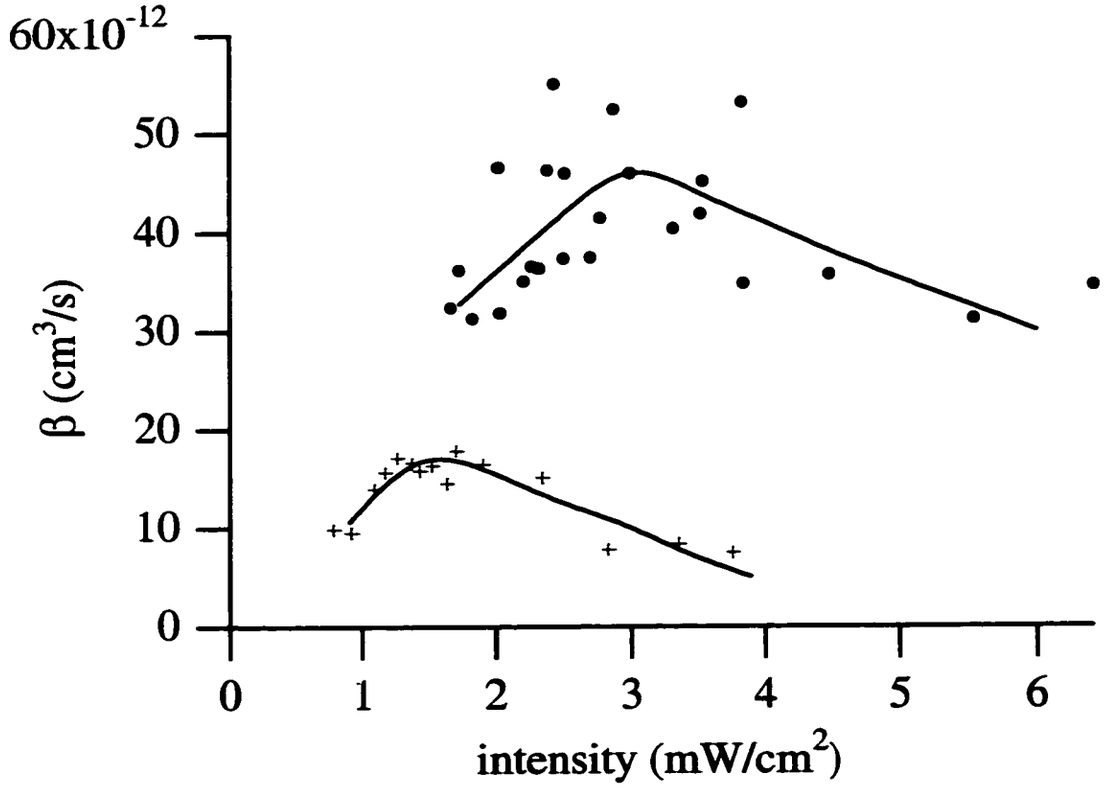

Figure 4.8: Loss rates taken at larger detunings. The +'s indicate the data at -1.5Γ detuning and circles indicate the data at -2Γ detuning. The larger detuning data show an intensity dependence for low intensities similar to the $\Delta = -1\Gamma$ data.

4.4 Hyperfine Pumping Results

In addition to measuring the loss rates as a function of trap laser intensity, the loss rates as a function of hyperfine pumping laser intensity was also measured. The hyperfine pumping laser repumps atoms that are in the the untrapped F=1 hyperfine level to the trapped F=2 hyperfine level where they can be recaptured by the trap. Atoms can be transferred to the lower hyperfine level through collisions and are also slowly pumped into this level by the trap laser. Decreasing the hyperfine pumping intensity allows the atoms to spend more time in the untrapped level before they are repumped. During that time the atoms are moving, and if they move far enough while in the lower hyperfine level, they can escape the trap.

These trap loss measurements were performed using the same technique used for the other measurements. The trap was first loaded at high intensity with hyperfine pumping intensity also set to its maximum. After the trap was fully loaded the both the trap and hyperfine pumping intensities were changed. Trap loss measurements were taken at four different values of the trap laser intensity, 0.7 mW/cm^2, 1.6 mW/cm^2, 4 mW/cm^2, and 10 mW/cm^2. The laser detuning was kept at one linewidth and the magnetic field gradient was at 10 G/cm. Prior to taking the trap loss data, the hyperfine pumping intensity was decreased until the excited state fraction was affected. This effect was measured by comparing the ratio of the fluorescence for a high intensity trap to the fluorescence at the low intensity. The minimum intensity for taking data was chosen so that fluorescence ratio remained constant. While taking the trap loss data the hyperfine pumping intensity was held above that intensity. The trap performance was not affected by the decrease in hyperfine pumping, meaning that any observed effect is caused by collisions and not the slow pumping of the trap laser.

The results of these measurements are shown in figure 4.9. Clearly, the loss rates are

unaffected for a large reduction in the hyperfine pumping, however, at approximately .12 mW/cm^2 the loss rates increase for all but the lowest trap laser intensities. The trap laser intensity 0.7 mW/cm^2 corresponds approximately to the peak in the loss rate as a function of trapping intensity, and thus the loss rates for that intensity are much higher overall than the other intensities. Similarly, at 4 mW/cm^2 the trap loss rate is nearly a minimum, and the measured loss rates are lower than at the other intensities. The rapid decrease in the loss rate with hyperfine pumping intensity indicates that atoms are ending up in the lower hyperfine level. A similar measurement was taken in the previous rubidium trap loss experiment.[Gensemer 97] They interpreted the increase in loss rate as the hyperfine pumping was decreased as an indication that spin exchange collisions were occurring. In that experiment, however, the effect of reducing the hyperfine pumping was considered only for a single trap laser intensity in the regime where the trap depth cannot recapture spin exchange collisions.

The data taken at 10 mW/cm^2 shows the same behavior as the 1.6 and 4 mW/cm^2 data. At 10 mW/cm^2 the trap is quite deep as compared to the lower intensities. If the increase in loss were demonstrating that spin exchange collisions were occurring, the 10 mW/cm^2 data should not show as strong a dependence on hyperfine pumping intensity. An atom that has gained one unit of ground state hyperfine splitting would have to travel further to escape the trap at 10 mW/cm^2 as compared to 1.6 mW/cm^2. That effect would cause the loss rate to increase at lower hyperfine intensity for 10 mW/cm^2 as compared to 1.6 mW/cm^2. In fact, the rates all seem to increase at nearly the same intensity.

A second interpretation of the data is that a radiative escape process is transferring atoms to the untrapped hyperfine level. The continuous range of energies imparted to atoms in this process would allow atoms to gain much more energy than in a spin exchange process. Reducing the hyperfine pumping intensity allows the atoms to move

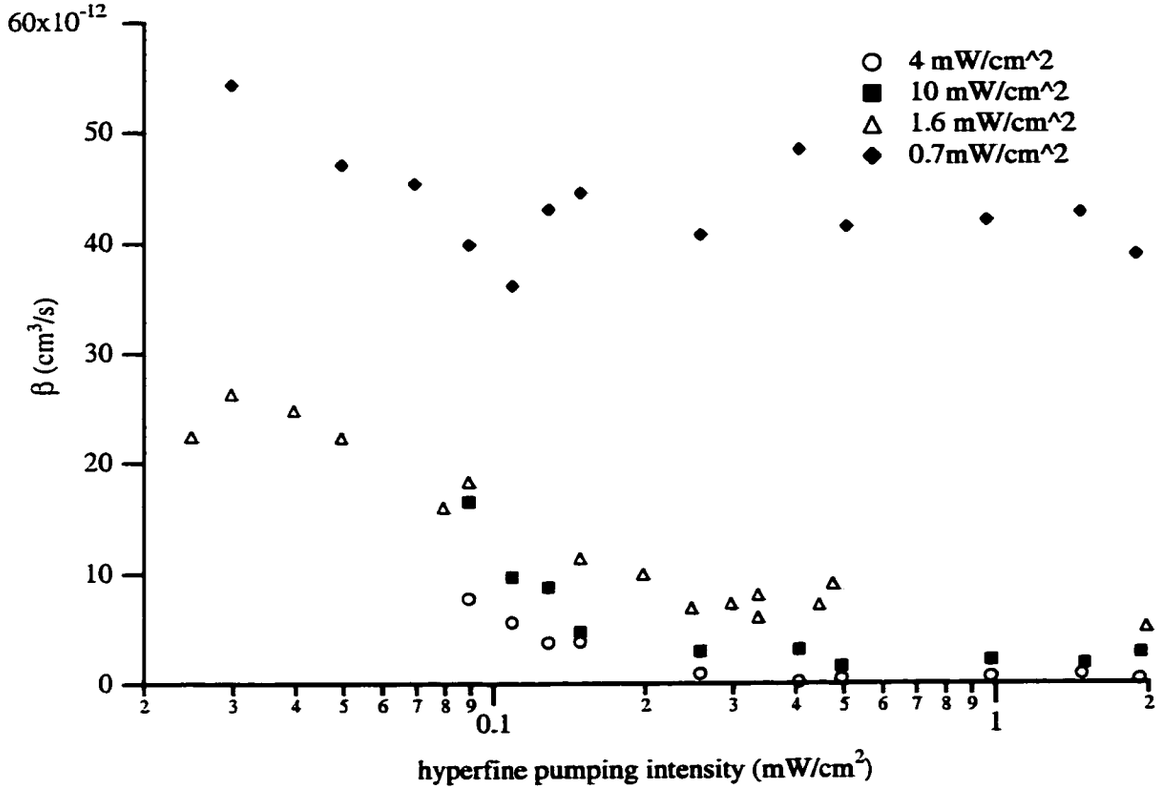

Figure 4.9: Loss rates as a function of hyperfine pumping intensity for 4 different trap laser intensities. For all data the magnetic field gradient was 10 G/cm and the trap laser detuning was -1Γ. The three highest trap laser intensities show a similar decrease in loss rate with intensity. The 0.7 mW/cm^2 data is near the peak of the loss rate as a function of intensity and thus the overall loss rates are higher. The intensity dependence shows that atoms are ending up in the lower hyperfine level, but does not imply that spin exchange is responsible for the transfer to that level.

unopposed by the trapping forces for a longer time before being repumped into the trapped state, and thus the effect can be viewed as decreasing the effective trap depth once the hyperfine pumping is reduced below some intensity. Atoms that are transferred to the lower hyperfine level with energy just below the trap depth are thus able to escape the trap once the hyperfine pumping has been reduced below the point for which the trap depth is affected.

4.5 Summary of results

The trap loss measurements as a function of intensity compare quite well with the previous measurements both in the overall shape of the data as well as the values for the loss rates. This data has been taken at much lower intensities than the previous data. At these low intensities the loss rate does not reach a plateau, as was previously suggested, but rather decreases with decreasing intensity. At one linewidth detuning the trap loss rate peaks at low intensity at a value of $\sim 5 \times 10^{-11}$ cm^3/s. For larger trap laser detunings the data had the same shape, however the signal to noise was not as good. Further, the effect of the hyperfine pumping intensity on the loss rate does show that the trap loss is due to collisions for which one or both atoms end up in the lower hyperfine level. In the next chapter three possible mechanisms that could be responsible for the intensity dependence at low intensity as well as the high loss rate as compared to the double BEC result are discussed and analyzed.

Chapter 5

Discussion and Interpretation

5.1 Introduction

In this section potential processes that could account for the difference between the MOT and BEC loss rates as well as the intensity dependence of the trap loss rate for low intensities are described. Any potential process should meet three conditions: the process should provide an intensity dependence of the loss rate, the peak loss rate should be on the order of 10^{-11} cm^3/s, and the energy associated with the process should be comparable to the ground state hyperfine splitting. The low ^{87}Rb BEC spin exchange rate is a result of a near cancellation of the singlet and triplet phase shifts. One explanation for the discrepancy between the MOT and BEC results is that the light disrupts this balance. Another possible process is an excited-state spin exchange process. If the change in hyperfine level took place in an excited state process rather than in a ground state process, the presence of the trapping light would play a role in the collision. The Connecticut group has also measured an increase in excited state collisional trap loss caused by a flux enhancement process. Flux enhancement is an increase in pairs of atoms at close range due to acceleration on an attractive potential.

5.2 Phase Balance

The very low spin exchange rate measured in the double Bose condensate experiment was theoretically reconciled as a serendipitous coincidence of the singlet and triplet scattering lengths.[Julienne 97, Burke 97, Kokkelmans 97] The near-perfect match between the two scattering lengths led to destructive interference between the accumulated phases, suppressing the spin-exchange rate. One interpretation of an intensity dependence of the spin exchange process at very low intensity is that the presence of the light mixes some of the excited $1/R^3$ potential in with the ground $1/R^6$ potential. This mixing could potentially upset the delicate balance between the phases if the singlet and triplet phases are affected differently.

In order for the phase balance to be disrupted, there must be a resonance between the ground and excited states at the interatomic separation for which the exchange interaction becomes important. This separation, where the exchange interaction is comparable to the hyperfine interaction is $22a_o = 11.6$ Å.[Julienne 97] The excited state potentials can be determined using the Movre and Pichler equations.[Movre 77] Those potentials are shown in figure 5.1. In order to determine the existence of a resonance, the energy of the potentials has been shifted such that the $P_{3/2}$ states asymptotically go to zero.

Next, the attractive nature of the ground state potential can be included using the Krauss and Stevens potentials for rubidium.[Krauss 90] The the energy of the pair of atoms in the interaction region is increased by the attractive potential. At 11.6 Å this energy increase is ~1 meV. The ground state potential has been superimposed on the excited state potentials in figure 5.2. A resonance exists where the ground state potential intersects one of the excited potentials. A resonance can be seen at 11.4 Å with the 0_g^+ level of the $5P_{1/2}$ state. Thus it would seem that the phase disruption is

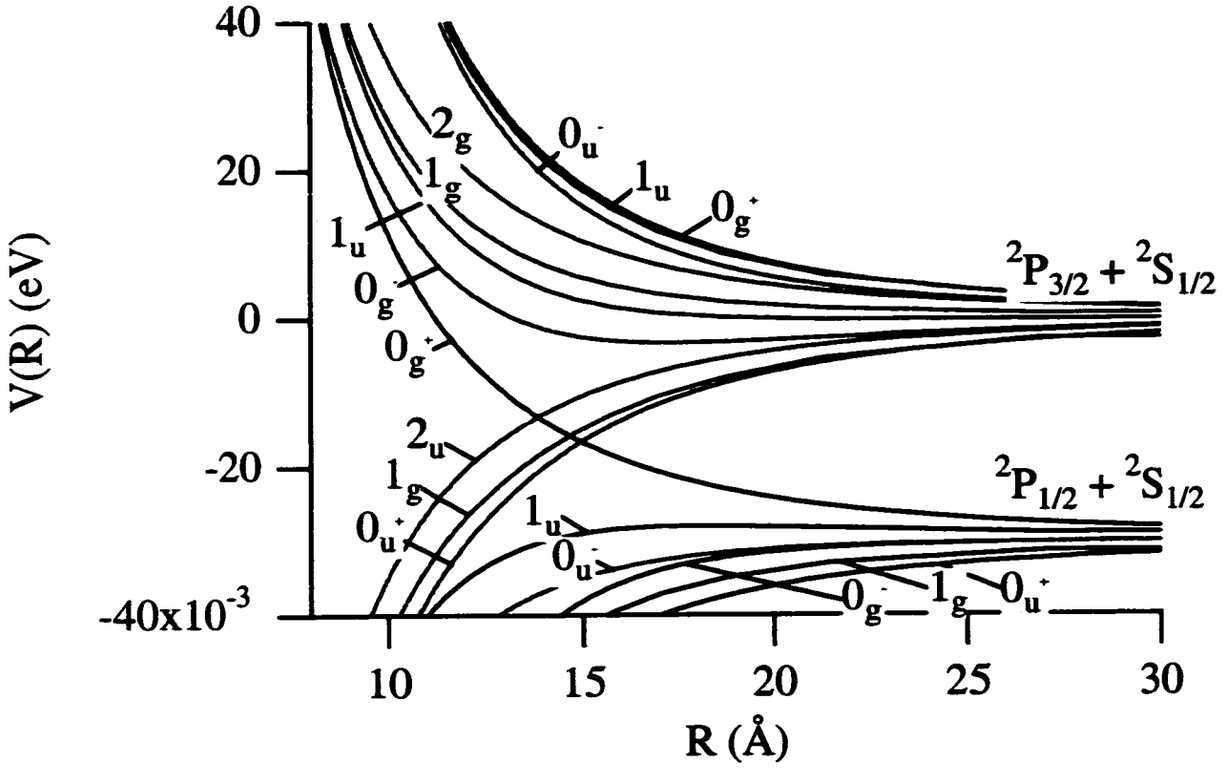

Figure 5.1: Excited state potentials as calculated by [Movre 77].

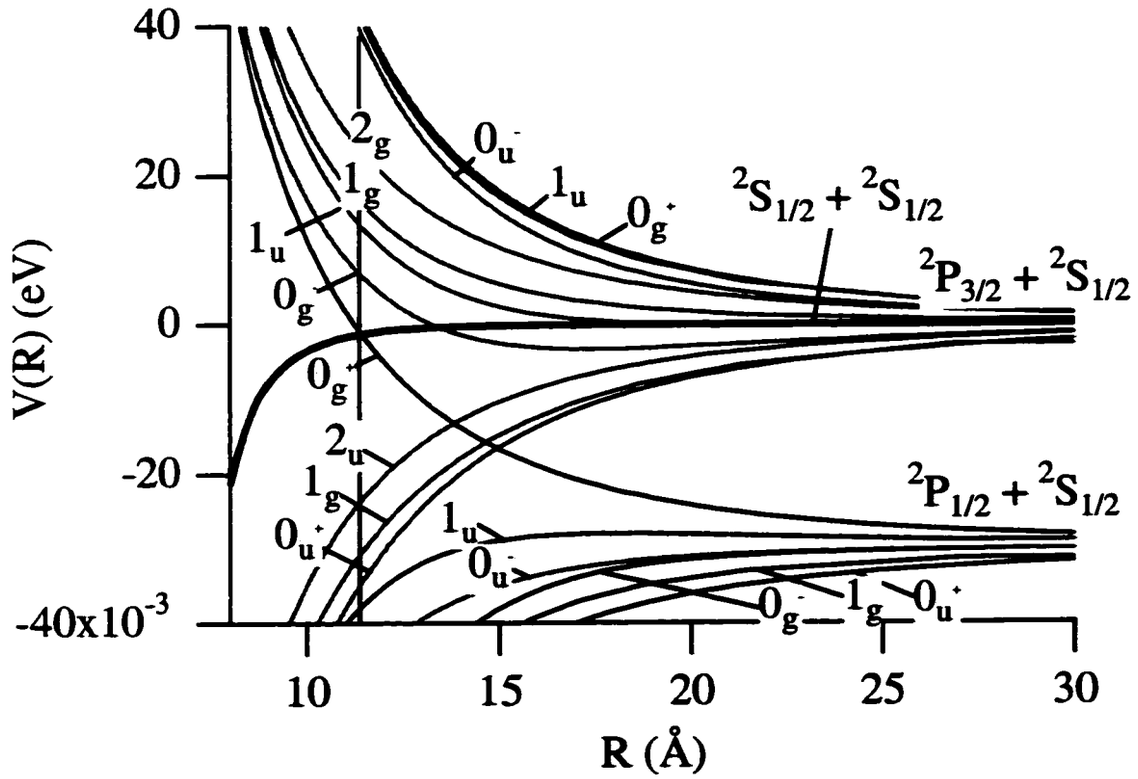

Figure 5.2: Ground and excited potentials in the region where the exchange interaction is comparable to the hyperfine splitting. The ground state potential is resonant with the excited state 0_g^+ potential at 11.4 Å.

possible.

5.3 Excited State Process

Another process that would show intensity dependence is an excited state spin exchange process similar to fine-structure changing collisions. The process is shown in figure 5.3. The collision would proceed as a standard excited state collision in which the colliding pair absorbs a photon and is transferred to an excited state potential. In this case mixing of potentials would result in the excited pair undergoing a curve crossing to a potential for which the ground state atom changes its hyperfine level rather than the

excited atom changing fine structure levels:

$$5P_{3/2} + 5S_{1/2}(F = 2) \rightarrow 5P_{3/2} + 5S_{1/2}(F = 1) \tag{5.1}$$

After radiating back to the ground state, the atoms would have gained kinetic energy equal to the ground state hyperfine splitting. Thus, the characteristic energy would be identical to that of a typical ground-state spin exchange collision, but the loss rate would have an intensity dependence since it is an excited state process. One of the most obvious characteristics of this process is that unlike ground-state spin exchange, only one atom can change hyperfine levels. Thus the energy imparted to the atoms can only be one unit of hyperfine splitting.

The question of whether one or two atoms changes hyperfine level has been investigated in terms of the trap depth. In 1996 Hoffmann *et al.* used repulsive trap loss collisions to measure the trap depth for the two isotopes of rubidium.[Hoffmann 96] The ground and excited state potentials are depicted as dressed states in figure 5.4. A high intensity catalysis laser was tuned above the atomic resonance with detuning Δ. This laser was used to excite atoms from the ground state to one of many repulsive excited state molecular potentials. Once transferred to an excited potential the atoms repel one another and each gain kinetic energy equal to $h\Delta/2$. As in other trap loss experiments, if the kinetic energy gained by the atoms is greater than the trap depth, the atoms will be lost from the trap. The trap depth can be inferred by observing the trap loss rate as a function of catalysis laser detuning.

The trap parameters for the MOT were set to be similar to the Connecticut experiment. The catalysis laser detuning was varied from 0 to 100 GHz, and the loss rate was measured as a function of the catalysis laser detuning. Their results are shown in figure 5.5. The loss rate increases sharply with detuning until $h\Delta > 2E_t$ where E_t is the trap depth. As the detuning is increased further, the loss rate begins to decrease.

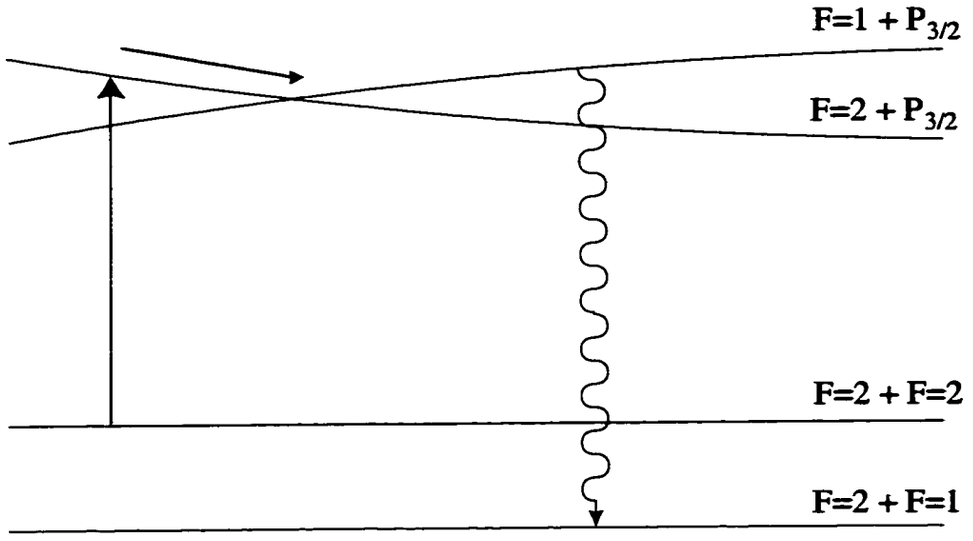

Figure 5.3: Process for excited state hyperfine changing collision. The atoms absorb a photon at close range and are transferred to an excited state potential. The atoms then go through a curve crossing for which the ground state atoms changes hyperfine levels. When the atoms reradiate one of the atoms is inthe lower hyperfine level.

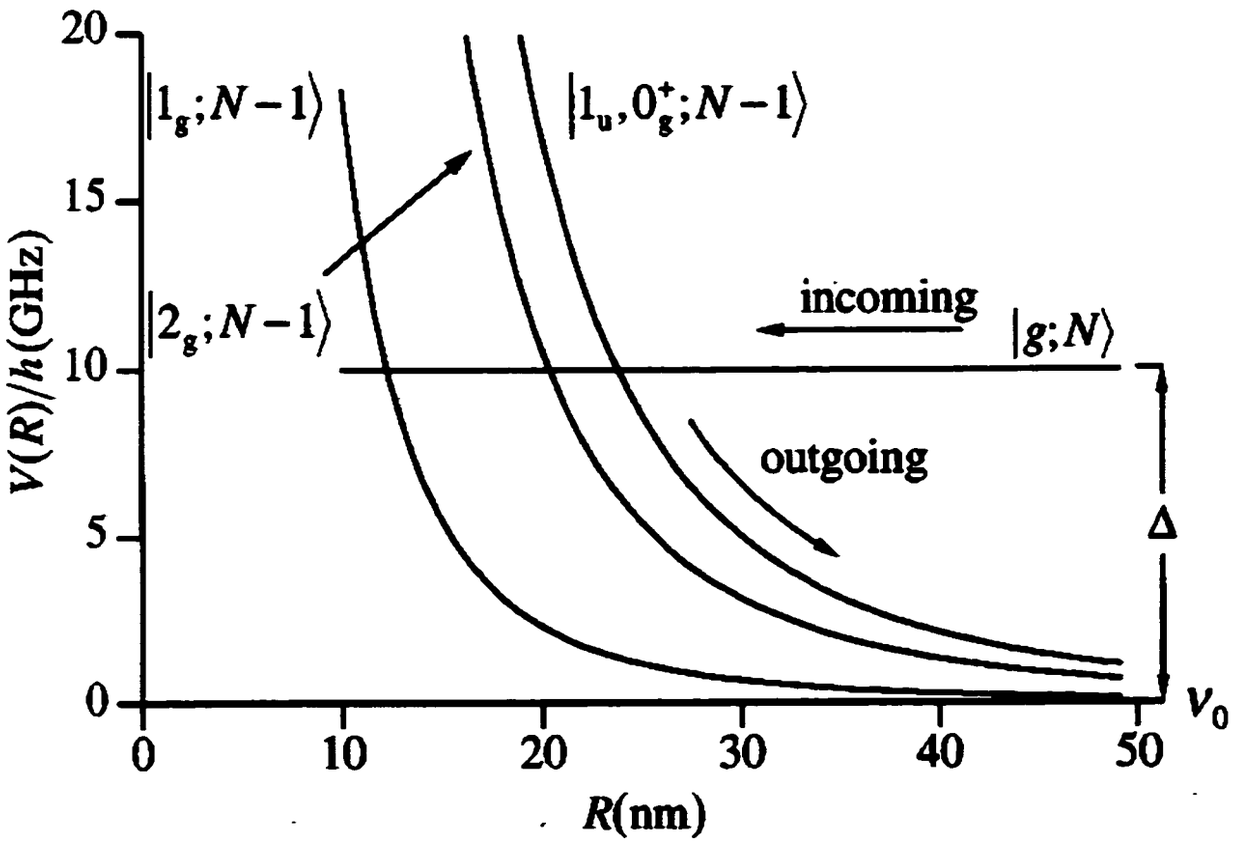

Figure 5.4: Process for excitation to repulsive states. The energy levels are shown as dressed states. The atoms approach on the ground state potential until the catalysis laser is resonant with one of the excited potentials. Once on a repulsive potential the atoms accelerate away from each other, gaining total kinetic energy equal to $h\Delta$.

The repulsive trap loss cross section is given by $\sigma = \pi R^2 f$ where R is the interatomic separation for which the catalysis laser is resonant and f is the excitation probability. As the detuning is increased, the resonant separation, R, becomes smaller, decreasing the loss rate.

The data show that for both isotopes the detuning must be greater than 15 GHz in order for appreciable trap loss. Because the atoms share the collision energy, the trap depth was inferred to be at least 7.5 GHz. The ground state hyperfine splitting in ^{87}Rb is 6.8GHz, thus for a spin exchange collision in which only one atom changes hyperfine

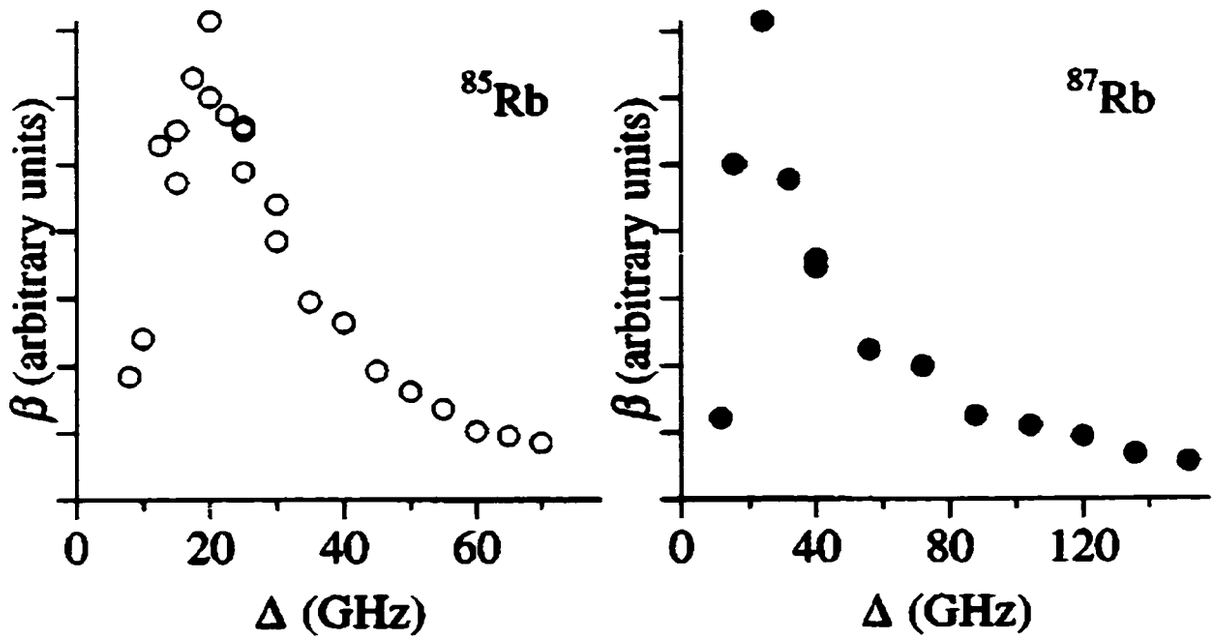

Figure 5.5: Loss rate as a function of catalysis laser detuning for repulsive states. The detuning must be larger than 15 GHz in order to produce appreciable trap loss.

levels, each atom gains 3.4 GHz in kinetic energy. For a trap depth of 7.5 GHz, those atoms would not be able to escape the trap. The trap depth measurements indicate that the spin exchange collisions must result in both atoms changing hyperfine level. Under those conditions, an excited state process for which only one unit of hyperfine splitting is released would not result in trap loss. The requirement that both atoms change hyperfine level argues against an excited state trap loss process.

5.4 Flux Enhancement

A third explanation of the low-intensity behavior of the trap loss is flux enhancement. This process was first reported by the Connecticut group in 1996.[Sanchez-Villicana 96]. The idea behind flux enhancement is that the presence of the trap laser excites atom pairs and accelerates them due to the attractive nature of the excited molecular poten-

tial. The acceleration provides an enhancement in flux of ground state atoms reaching close range. Although their work explored the effect of flux enhancement on excited state collisions, it should also play a role in ground state collisions.

5.4.1 Excited State Flux Enhancement Experiment

In the Connecticut experiment a probe laser with a large negative detuning compared to the trap laser was used in addition to the trap laser to excite the atoms at very close range, on the order of 35 nm. They measured the loss rate in three different situations: with the trap laser alone, with the probe laser alone, and with both lasers. The trap laser intensity was set such that ground-state collisions could not escape. With the trap laser alone, the number of atoms reaching close range was presumably increased, however when the atoms reached close range, they were in the ground state and thus very little trap loss was observed. With the probe laser alone, very few atoms reached close range, however any that did were excited by the probe and lost from the trap due to excited state collisions. With both lasers present, they observed a cooperative effect in that the trap loss was larger than the sum of the loss rates due to the individual lasers.

Flux enhancement affects the collisions dynamics by allowing atoms with higher initial angular momentum to be drawn in to close range. Quantum mechanically this acceleration on the excited state potential allows atoms to overcome the centrifugal barrier, increasing the number of partial waves that contribute to the collision. In addition, flux enhancement gives the L=0 contribution more energy, so the phase shifts have to be evaluated at higher energy.

5.4.2 Langevin Analysis of Flux Enhancement

The effect of higher angular momentum atoms being drawn in to close range has been examined classically using a Langevin analysis. To do this, the effect of acceleration on the velocity and impact parameter were first determined. Then, the collision rate as a function of time spent on the excited potential could be calculated by requiring that the modified impact parameter be equal to the Langevin impact parameter.

The interaction is shown in figure 5.6. Consider a pair of atoms with initial velocity $\mathbf{v}$ in the presence of near resonant light with a detuning $\Delta = \omega - \omega_o$. For negative laser detuning the attractive potential $U = -C_3/R^3$ is resonant at the Condon point, $R_C = (-C_3/\hbar\Delta)^{1/3}$. At R_C the pair is transferred to the attractive excited state potential, accelerating the pair, which gives a change in the velocity Δv_r directed along a line between the two atoms. The velocity increase Δv_r can be related to the time, τ, spent on the the excited potential using $F = -\partial U/\partial r = \mu \Delta v_r/\tau$ which gives

$$\Delta v_r = \frac{3C_3}{\mu R_c^4}\tau \tag{5.2}$$

where μ is the reduced mass. We have used the values $C_3 = 80$ eVÅ and $R_c = 1000$Å. The new velocity, $\mathbf{v_{new}} = \mathbf{v} + \mathbf{\Delta v_r}$, results in a new impact parameter for the collision, b_{new}.

Figure 5.6 gives the geometry necessary for relating the original impact parameter b_o to b_{new}. We begin by noting from Fig. 5.6a that b_{new} and b_o can be written as

$$b_{new} = R_C \sin(\theta - \phi), \tag{5.3}$$

and

$$b_o = R_C \sin\theta. \tag{5.4}$$

Figure 5.6b shows the sum of the velocities and provides the relation

$$\Delta v_r \sin(\theta - \phi) = v \sin\phi. \tag{5.5}$$

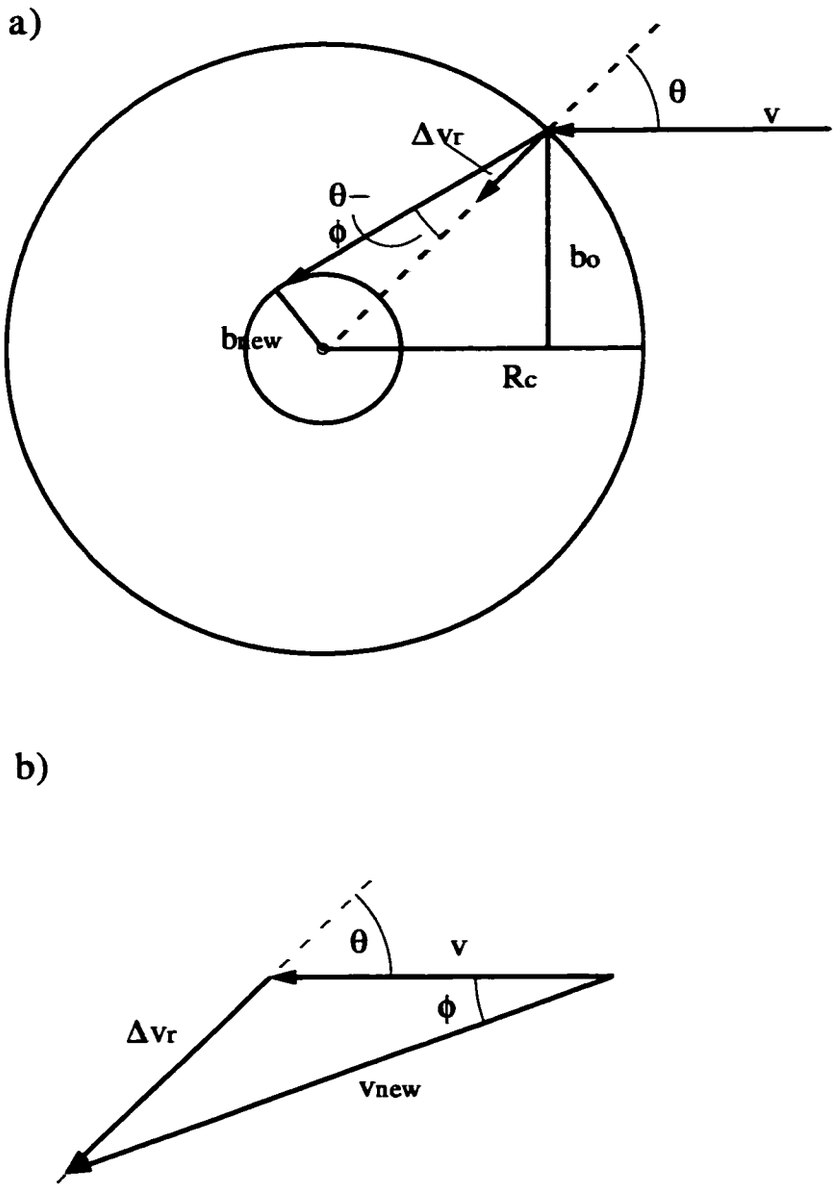

Figure 5.6: Geometry for impact parameter calculations showing the effect of excitation on the velocity and impact parameter. The pair is transferred to the excited potential at the Condon radius, R_C.

From this relation we can rewrite Eq.(5.3) as

$$\sin\phi = \frac{\Delta v_r}{v}\frac{b_{new}}{R_C}. \tag{5.6}$$

In addition, Eq.(5.5) can be rewritten using a trigonometric identity as

$$\sin\phi = \frac{\frac{\Delta v_r}{v}\sin\theta\cos\phi}{1+\frac{\Delta v_r}{v}\cos\theta} \tag{5.7}$$

Eq.(5.7) is linear for small $\sin\theta$ so the cosine dependences can be set to 1. Equating Eqs.(5.7) and (5.6) we find

$$\sin\theta(\frac{\frac{\Delta v_r}{v}}{1+\frac{\Delta v_r}{v}}) = \frac{\Delta v_r}{v}\frac{b_{new}}{R_C} \tag{5.8}$$

Thus

$$\sin\theta = \frac{b_{new}}{R_C}(1+\frac{\Delta v_r}{v}), \tag{5.9}$$

and

$$b_o = b_{new}(1+\frac{\Delta v_r}{v}). \tag{5.10}$$

The effect of atoms being drawn in is described by the Langevin impact parameter. This impact parameter is defined as the interatomic separation for which the incident kinetic energy is equal to the $1/R^6$ potential energy. This definition essentially requires that the atoms have less energy than the $1/R^6$ potential in order to be affected by that potential. The Langevin impact parameter is given by

$$b_{Lang} = [\frac{2C_6}{\mu v_{tot}^2}]^{1/6} \tag{5.11}$$

where C_6 is the coefficient for the $1/R^6$ potential. Combining the Langevin effect and the increase in velocity, a spin exchange collision can occur if b_{new} is less than or equal to the Langevin impact parameter. Thus the maximum initial impact parameter, before excitation, for which the atoms will reach close range can be found by replacing b_{new} by b_{Lang} in Eq. 5.10:

$$b_{max} = b_{Lang}(1+\Delta v_r/v). \tag{5.12}$$

The collision rate can then be found as

$$\begin{aligned} \beta &= \int_0^\infty vp(v)dv \int_0^{b_{max}(v)} 2\pi b_o db_o \\ &= \pi \int_0^\infty vp(v)dv b_{max}^2(v) \end{aligned} \tag{5.13}$$

where b_o is the initial impact parameter and p(v) is a Maxwell-Boltzmann distribution.

Calculating this integral as a function of time spent on the excited potential gives an estimate of the classical effect of the acceleration on increasing the collision rate. For $\tau = 0$, we find a value for β of 4.3×10^{-11} cm^3/s , corresponding to the case of no excitation. For $\tau = 1$ natural lifetime we get $\beta = 9.2 \times 10^{-11}$ cm^3/s. Thus classically we see a factor of 2 increase in the collision rate as a result of this effect. Using the Langevin impact parameter we can calculate the angular momentum for a collision at 100 μK:

$$\hbar L = \mu v b_{Lang} = 1.1\hbar. \tag{5.14}$$

This results suggests that we should treat the problem quantum mechanically, and consider the effect of flux enhancement on the different partial waves.

5.4.3 Quantum Mechanical Treatment

In terms of angular momentum, the effect of flux enhancement is to make it easier for higher partial waves to overcome the centrifugal barrier. Acceleration on the excited state potential alters the velocity distribution. To explore the effect this has on the collision rate we first must determine the velocity distributions as a function of time spent on the excited potential.

The final velocity, after acceleration, can written as $v_f = v_o + at$ where t is the time spent on the excited state potential, and a is the acceleration, given by

$$a = \frac{3C_3}{\mu R^4} \tag{5.15}$$

where R is the interatomic separation for which the trap laser is resonant with the excited potential. The time on the excited potential has a distribution

$$p(t) = \frac{1}{\tau} e^{-t/\tau} \tag{5.16}$$

where τ =27 ns, the excited state natural lifetime. Because the time spent in the excited state has a distribution, the final velocity, due to acceleration also has a distribution:

$$p(v) = \begin{cases} \frac{1}{a\tau} e^{-(v-v_o)/a\tau} & v > v_o \\ 0 & v < v_o \end{cases} \tag{5.17}$$

In addition we have to allow for the Maxwell-Boltzmann distribution of initial velocities, so the total velocity distribution is

$$P(v_f) = \int dv_o p(v_o) p(v_f) \tag{5.18}$$

$$= \frac{1}{a\tau} \left(\frac{2\mu^3}{\pi T} \right)^{1/2} \int_0^{v_f} dv_o e^{-\mu v_o^2/2T} v_o^2 e^{-(v_f - v_o)/a\tau} \tag{5.19}$$

The modified distributions are shown for various times, expressed in terms of the natural lifetime, in figure 5.7. The initial temperature used in the Maxwell-Boltzmann distribution was 100 μK in each case. The $\tau = 1$ distribution has been used in the remaining calculations because it corresponds to the natural lifetime of the excited state. The mean velocity is 22.2 cm/s for the unmodified case as compared to 36.4 cm/s for one natural lifetime.

To estimate the effect that the modified velocity distribution would have on the higher partial waves, the velocity associated with the centrifugal barrier for each of the partial waves is needed. The position and velocity of the barriers were found using Krauss and Stevens potentials [Krauss 90] and adding centrifugal potential $\frac{\hbar^2 l(l+1)}{2\mu R^2}$ for each partial wave. The values for the barrier velocity, v_{bar}, are given in the table in figure 5.8. The effect of the enhancement is then found by integrating the modified

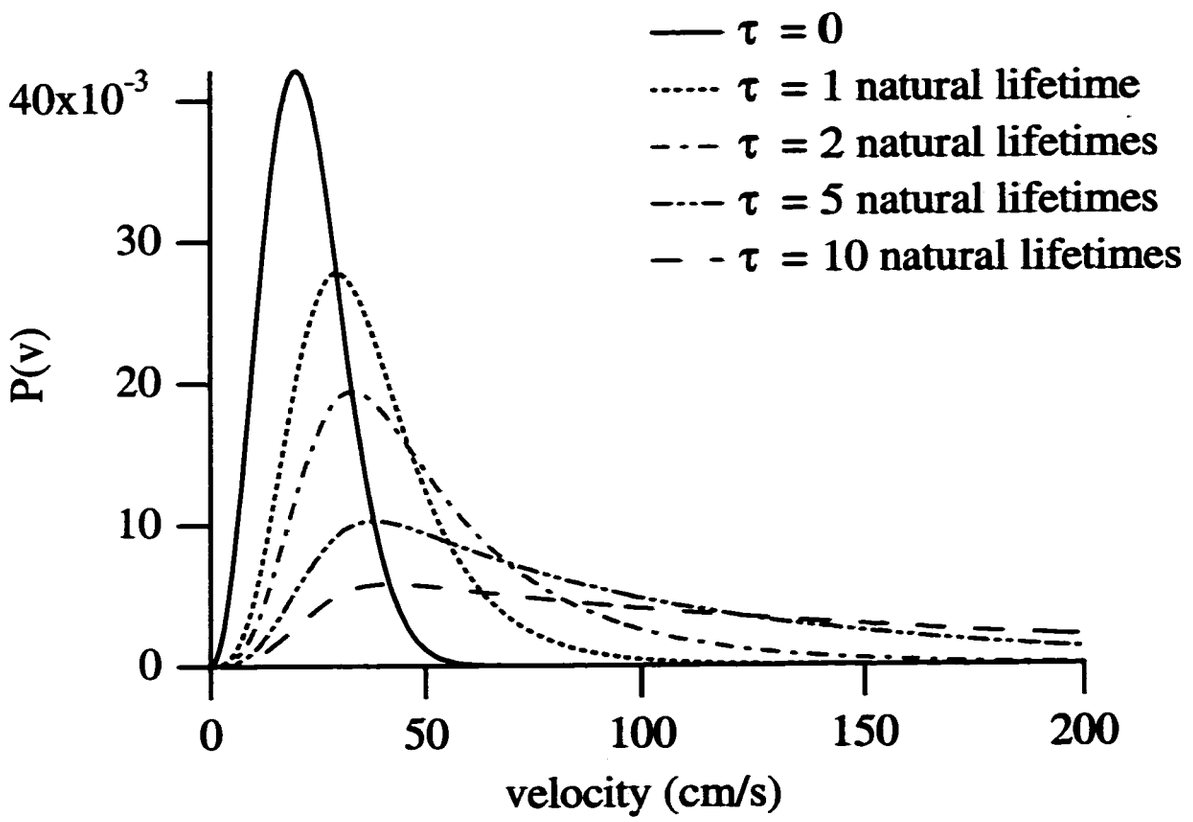

Figure 5.7: Modified velocity distributions. The initial ($\tau = 0$) distribution is a Maxwell-Boltzmann distribution at 100 μK. The other distributions include the effect of acceleration for various times τ on the excited potential.

	τ=0	τ =1	τ =2	τ =5	τ =10
L=1 v_{bar} = 17.9 cm/s	0.664	0.906	0.948	0.977	0.987
L=2 v_{bar} = 40.8 cm/s	0.0373	0.341	0.556	0.781	0.881
L=3 v_{bar} = 65.3 cm/s	6.08×10^{-5}	0.064	0.239	0.556	0.743

Figure 5.8: Table of values comparing integrated velocity distributions. The distributions in fig. 5.7 have been integrated from v_{bar} to ∞ for each of the partial waves.

velocity distribution from v_{bar} to infinity. We can then compare the integrated distributions for various times, τ, on the excited potential to the integrated distribution for $\tau = 0$. The integrated distributions are also shown in the table. From these rough calculations we see that there is a significant p-wave contribution even without the acceleration. In addition, the acceleration increases the d-wave contribution by an order of magnitude. Finally, we see that the f-wave contribution remains quite small because the barrier velocity is too large to contribute at these temperatures.

To get values for the cross-sections and rate coefficients for the higher partial waves, we need to know the phase shifts for the singlet and triplet potentials. The phase shifts were determined using a program that integrated the Schrödinger equation for a given kinetic energy using a fit to the Krauss and Stevens potentials for rubidium. In the asymptotic limit, the wave function can be written as

$$\psi(r) = A\sin(kr - \frac{l\pi}{2} + \phi_l). \tag{5.20}$$

In addition, the derivative is

$$\psi' = Ak\cos(kr - \frac{l\pi}{2} + \phi_l). \tag{5.21}$$

Thus the phase shift can be extracted using

$$\phi_l = \tan^{-1}\left(\frac{k\psi}{\psi'}\right) - (kr - \frac{l\pi}{2}). \tag{5.22}$$

Once the phase shifts have been calculated as a function of incident kinetic energy, the cross section can be determined using

$$\sigma_l = \frac{\pi}{k^2}(2l+1)\sin^2(\phi_s - \phi_t). \tag{5.23}$$

Finally the cross-section and the modified velocity distribution can be used to calculate the rate coefficient:

$$\beta = \int_0^\infty vP(v)\sigma(v). \tag{5.24}$$

The phase shifts can be modified by adjusting the fit parameter that controls the strength of the repulsive barrier in the exchange potential. The Krauss and Stevens potentials were recast as direct and exchange potentials so that the strength of the exchange interaction could be adjusted by modifying only one potential. Both the direct and exchange potentials were fit to the equation

$$V(r) = -a_0 e^{-r/a_1} + a_4 e^{-(r-a_6)^2/a_5^2} - a_2\left(\frac{1-e^{-a_3 r}}{r}\right)^6 \tag{5.25}$$

The values for the coefficients a_i are given in figure 5.9. The strength of the exchange potential can be controlled by modifying the parameter a_4. We adjusted this parameter in order to get good cancellation of the s-wave phases, as required by the theoretical interpretation of the double Bose condensate result.

Calculating the rate coefficient for the s-wave contribution using the $\tau = 1$ modified velocity distribution gave a value for β of 9.24×10^{-14} cm^3/s. This number is in fairly good agreement with the value obtained using Williams' calculations of 2.9×10^{-13} cm^3/s.[Williams 98] Williams' rate coefficients shown as a function of energy in figure 2.6 were not averaged over a thermal distribution. To do this averaging, his

	a0	a1	a2	a3	a4	a5	a6
Direct	7.4043	1.2768	2691	0.1416	8.8056	2.2505	0
Exchange	2.0444	0.95583	0	0.11846	1.0445	-2.4808	2.5714

Figure 5.9: Table of coefficients for the exchange and direct potentials. The equation for the potentials is given in Eq. (5.25).

data was multiplied by the modified velocity distribution and then integrated. All of the rate coefficients, including higher partial waves, are shown in figure 5.10 for both the case of flux enhancement ($\tau = 1$) and no flux enhancement ($\tau = 0$). The total rate coefficient, found by summing each of the contributions from the partial waves, is then 1.70×10^{-11} cm^3/s, for the case of flux enhancement, as compared to 9.0×10^{-12} cm^3/s without enhancement. Thus flux enhancement provides at least a factor of two increase in the rate.

To compare this result to the experimental data, the calculated rate coefficient must be multiplied by two to account for both atoms leaving the trap. The loss rate is then 3.4×10^{-11} cm^3/s which compares quite well with the peak observed loss rate of $\sim 5 \times 10^{-11}$ cm^3/s for one linewidth detuning. This treatment of flux enhancement assumes that all of the atoms are affected by the trap laser. Therefore, although the absolute numbers are in good agreement with the measured values, they should only be considered an estimate.

5.5 Summary

I have examined three mechanisms that could bridge the gap between the measured loss rates and the much lower theoretically predicted values. In addition each of the three

	τ=1	τ=0
Williams' s-wave	2.91 x 10^{-13} cm^3/s	2.13 x 10^{-13} cm^3/s
s-wave	9.24 x 10^{-14} cm^3/s	8.19 x 10^{-14} cm^3/s
p-wave	2.46 x 10^{-13} cm^3/s	1.51 x 10^{-13} cm^3/s
d-wave	1.65 x 10^{-11} cm^3/s	9.09 x 10^{-12} cm^3/s
f-wave	3.59 x 10^{-14} cm^3/s	4.83 x 10^{-17} cm^3/s
total	1.70 x 10^{-11} cm^3/s	0.90 x 10^{-11} cm^3/s

Figure 5.10: Table of values for β calculations with flux enhancement ($\tau = 1$) and without ($\tau = 0$).

processes depends on the presence of light which would further explain the intensity dependence observed at very low intensity. The process that appears least likely to be responsible for the discrepancy between the measured loss rates and those predicted theoretically is an excited state hyperfine changing collision process. Because that process would only result in one atom changing hyperfine levels, the trap depth would have to be weak enough for atoms with only one-half a unit of ground state hyperfine splitting to leave the trap. The trap depth measurements performed using the repulsive potentials show that the trap is too deep for such a collision to cause trap loss. Thus the excited state process is not likely to affect the trap loss measurements.

The other two processes, disruption of the phase balance and flux enhancement, appear to likely play in role in the collision dynamics for these low-intensity traps. The existence of a resonance between the ground state and a $5P_{1/2}$ hyperfine level at the interatomic separation for which the exchange interaction becomes important could

disrupt the delicate balance of the singlet and triplet phases that suppressed spin-exchange in the double BEC experiment. Thus the collision cross section, which goes as $\sin^2(\phi_s - \phi_t)$, will not show the strong destructive interference in the presence of the near-resonant laser light. Although the velocity and slope of the curve are such that excitation to this level is extremely rare, the resonance may allow for phase disruption.

Finally I have considered classical and quantum mechanical interpretations of flux enhancement. The presence of the laser light acts to accelerate atoms that are relatively far apart to closer range, increasing the flux available for spin-exchange collisions. In addition to increasing the available flux, the acceleration modifies the velocity distributions. Quantum mechanically the shift in the velocity distribution allows higher partial waves to overcome the centrifugal barrier. I have shown that the addition of higher partial waves in the loss rates increases the predicted loss rates to bring the predictions into close agreement with the measured values.

Chapter 6

Excited State Fraction

6.1 Introduction

In order to determine the minimum trap laser intensity for which the trap operation was not affected, the trap intensity was decreased to the minimum and then turned back up to the maximum to ensure that the number of atoms remained constant. This diagnostic for trap alignment was discussed in section 3.5. It was then determined that a similar technique could be used to measure the excited state fraction of the trap for arbitrary intensity. The excited state fraction is an important parameter in many MOT experiments. For trap loss experiments, knowledge of the excited state fraction is required to convert the trap fluorescence signal into a number of atoms. Recently ground state electron scattering cross-sections have been measured using a MOT as the target.[Schappe 95] To extend this technique to excited-state cross-sections, accurate determination of the excited state fraction is also required.

The excited state fraction, f_e, is given by

$$f_e = \frac{\frac{I}{2I_s}}{1 + \frac{I}{I_s} + 4\frac{\Delta^2}{\Gamma^2}} \tag{6.1}$$

in which I is the total trap laser intensity, I_s is the saturation intensity, Δ is the laser

detuning, and Γ is the natural linewidth. For high intensities f_e saturates at a value of 1/2, thus for experiments in this regime the excited state fraction is known. For low to moderate laser intensities, however, the parameter must be experimentally determined. Previously, the only direct method for measuring the excited state fraction was to use photoionization out of the excited state.[Dineen 92] In the process of creating a diagnostic to verify trap alignment at very low intensities, we developed a new method for easily measuring the excited state fraction.

6.2 Measurements

Aside from photoionization measurements, the standard technique for obtaining the excited state fraction for trapping experiments is to calculate it from equation(6.1) using measured values for the trap laser intensity and detuning. The problem with calculating the excited state fraction is in choosing an appropriate value for I_s. The saturation intensity is affected by the details of the trap. For example, the atoms experience polarization gradients and optical standing wave patterns. In addition, the atoms can arrange themselves in optical lattices under the right conditions. Our method provides a means to experimentally determine I_s, which allows the excited state fraction to be calculated using equation(6.1) without requiring knowledge of the details of the trapping region.

The measurements used to determine I_s were based on the technique used for verifying trap operation at low intensities. The trap was first loaded with the trap laser at a maximum intensity, I_{max}, with the maximum intensity equal to 14-15 mW/cm^2. After the trap was loaded, the trap laser intensity was rapidly changed to some lower value, I. Switching the intensity was done using a liquid crystal variable attenuator, described in chapter 3. During the switching time, the number of atoms in the trap

remained the same, however the level of fluorescence changed. The trap fluorescence was monitored with a photodiode, allowing us to measure the ratio P/P_{max} where P_{max} is the photocurrent for the full trap laser intensity and P is the photocurrent at the lower intensity. Because of saturation effects this ratio is not equal to the ratio of the laser intensities, I/I_{max}.

We measured the ratio P/P_{max} over a wide range of trapping intensities. As in the trap loss data, the intensity was not decreased below the point where the trap performance degraded. To determine I_s, the ratio R:

$$\begin{aligned} R &= \frac{P}{P_{max}} \\ &= \frac{I}{I_{max}} \left(\frac{1 + I_{max}/I_s + 4\Delta^2/\Gamma^2}{1 + I/I_s + 4\Delta^2/\Gamma^2} \right). \end{aligned} \tag{6.2}$$

was plotted as a function of I/I_{max}. The data was fit with I_s and Δ as free parameters. Using the measured frequency would allow Δ to be held constant, meaning the fit has only one free parameter, however allowing Δ to vary provides additional confidence in the values for I_s.

Sample data with $I_{max} = 14.2$ mW/cm^2 and $\Delta = -1\Gamma$ and $\Delta = -1.5\Gamma$ are shown in figure 6.1. A least squares fit to these data gives the values $I_s = 3.05$ mW/cm^2 and Δ = -1.02Γ, and $I_s = 3.23$ mW/cm^2 and Δ = -1.65Γ. The detunings agree quite well with the measured values, and the saturation intensity values are also very reasonable. For unpolarized rubidium atoms a rate equation analysis gives $I_s = 3.6$ mW/cm^2, while for fully optically pumped rubidium $I_s = 3.0$ mW/cm^2.

Once the saturation intensity has been determined, the excited state fraction can be calculated from equation 6.1. This method is much more straightforward to implement than a photoionization method. In addition, because Eq.(6.2) is written in terms of ratios of intensities, this method does not require absolute measurement of the intensity.

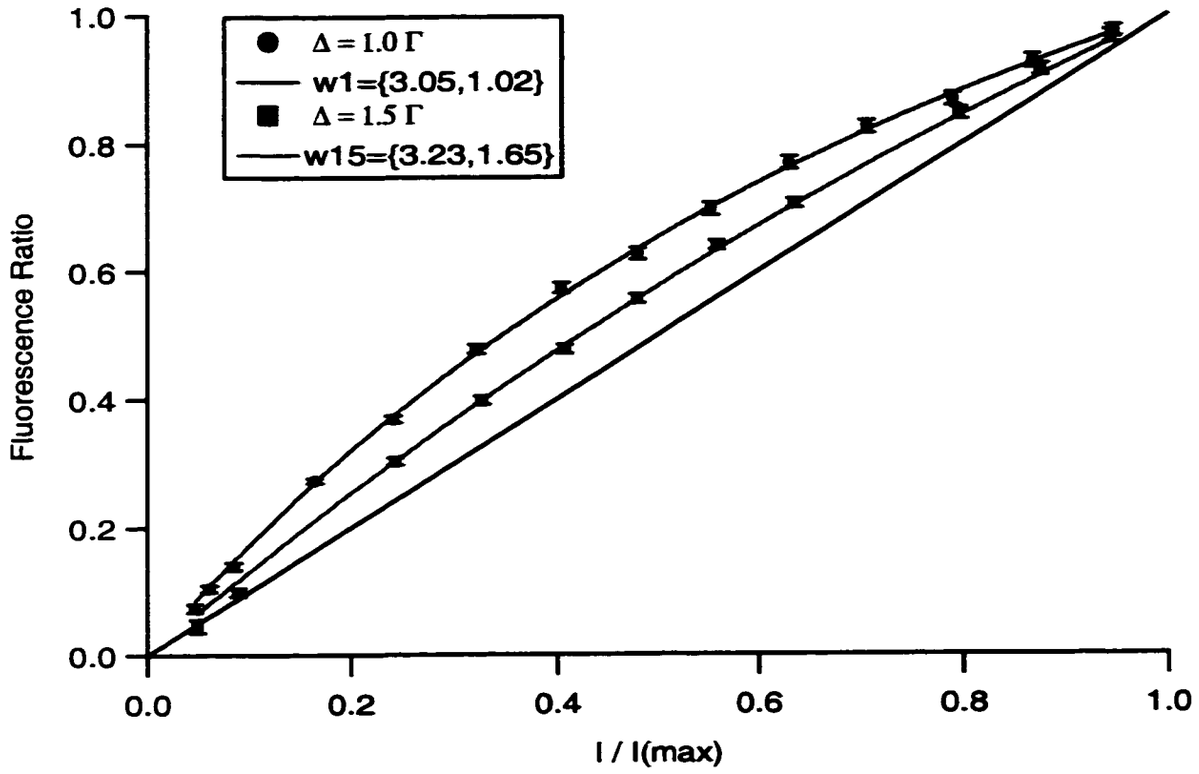

Figure 6.1: Excited state fraction data at two different laser detunings. The data was fit using two parameters, Δ and I_s. The values for Δ compare well with the measured values, and the values for I_s are also quite reasonable.

Appendix A

Cleaning Procedure for Ultrahigh Vacuum Parts

Stainless Steel UHV Cleaning Procedure

Procedure for thoroughly cleaning stainless steel after being machined, etc. (from a very dirty state). Absolutely nothing comes from the factory clean. Nothing! Even for electropolished parts it is a good idea to go through the Less-Anal procedure.

Anal procedure for filthy parts or extreme vacuum requirements:

1. Remove all obvious oil and grease from surface and holes in part. Vapor degrease only if part is in very oily/greasy condition. You can wipe with trichlorethane or even a shop solvent.

2. Use 1,1,1-trichlorethane (or accepted substitute) in ultrasonic cleaner for 3-5 minutes, or wipe it down carefully. Be sure holes are wetted/cleaned. Trichlorethane is a very good general organic solvent and dissolves most anything.

3. Prepare a solution of 25

4. Run the part under clean (preferably filtered if available) hot tap water, with a bowl underneath to catch and clean the part. Oakite is an alkaline soap solution, and

can be rather tenacious, so it much be rinsed very thoroughly.

5. Rinse part by pouring distilled water over it. Removes ions present in tap water.

6. If the part is small enough, let it sit or hang in boiling distilled water (over a heating plate) for 5-10 minutes.

7. Remove part and allow to dry; if part is intricate or has holes, assist with a pressure jet of dry bottled nitrogen. The hot metal evaporates the boiling distilled water and leaves very little residue, provided the part was throughly rinsed and the distilled water is pure.

8. You can end here with a final acetone wipe, then ethanol wipe. For viewports, end with an additional final acetone wipe. The ethanol evaporates slowly and tends to leave a bit of residue, possibly dust from the air. After wiping, blow off with dry nitrogen. Windows are really finicky, especially since you can see all the dust and particles, so assemble these to the chamber immediately after cleaning.

Less-anal procedure for cleaner or electropolished parts. Use on windows and on "lesser" UHV systems (10^{-9} torr or so):

1. Wipe with 1,1,1-trichlorethane and TX 304 natural wipes. These are pure cotton wipers and have no chemical residue, and claim to be lintless (they still leave a little lint, especially when used on sharp metal surfaces). From the factory, lots of black specks and dirt will come off with this solvent. Repeat wiping with new wipes until clean.

2. Now wipe with acetone. This can be a single or double wipe all over the surface. At this point, little or no visible residue should be on the wipe.

3. Wipe with methanol. This can be a single wipe, motly to remove residues which acetone does not work well on. For most stainless parts, you may end here by blowing off dust with dry nitrogen.

4. For windows, wipe once more with acetone, just like you would an optic. Best

bet is to use spectroscopic grade acetone, optical cloths, and forceps. Blow off with dry nitrogen (those optical cloths are really linty).

Copper UHV Cleaning Procedure

Procedure for thoroughly cleaning copper after being machined, etc. (from a very dirty state)

1. Remove all obvious oil and grease from surface and holes in part. Vapor degrease only if part is in very oily/greasy condition.

2. Use 1,1,1-trichlorethane (or accepted substitute) in ultrasonic cleaner for 3-5 minutes. Be sure holes are wetted. Change solution regularly if soiled (turns yellow, typically). Trichlorethane is a very good general organic solvent and dissolves most anything.

3. Prepare a solution of 25

4. Run the part under clean (preferably filtered if available) hot tap water, with a bowl underneath to catch and clean the part. Oakite is an alkaline soap solution, and can be rather tenacious, so it much be rinsed pretty thoroughly.

5. Rinse part by pouring distilled water over it. Removes ions present in tap water.

6. Let sit or hang in boiling distilled water (over a heating plate) for 30-seconds to 1 minute.

7. Allow to dry; if part is intricate, assist with a pressure jet of dry bottled nitrogen. For many applications, you can end here with a final acetone, then ethanol rinse.

8. Prepare an "assembly line" of solutions in beakers: 50

9. Soak the part in the HCl for 3-4 minutes. Allow to drip for 10 seconds, then soak in distilled water in ultrasonic cleaner for 1-2 minutes. Change this distilled water each time you dip a new part from the HCl into it. The HCl is a "pickling" solution which removes all the oxides and presents a fresh, clean Cu surface. The water dilutes and removes the HCl.

10. Using the ultrasonic cleaner, dip the part in acetone next for 1-2 minutes, then into the methanol for 1-2 minutes. The acetone removes the water and any final organics from from the water or acid. The methanol removes the acetone, which often contains long-chain organics which are hard to pump. Methanol is very clean and easy to pump away.

11. Package the part, put into a dessicator, or stored under nitrogen. This is a clean surface and should not oxidize very quickly.

12. If the part has small holes, it is often a good idea to blow dry nitrogen into them each time you change solutions (except after the HCl). Even the ultrasonic cleaner doesn't mix the old solution and the new solutions very well each time with a small hole blocking the flow.

Appendix B

Data Analysis Functions for IGOR

```
#pragma rtGlobals=1 // Use modern global access method.


Function /D Thadexp3(w,p)
Wave /D w; Variable /D p

if (w[2] < 0)
return -99999
endif
if (w[3] <0)
return -99999
endif

  return  w[0]+w[4]+1/((1/(w[1]-w[4])+w[2]/(w[3]+2*w[2]*w[4]))
*exp((w[3]+2*w[2]*w[4])*p)-w[2]/(w[3]+2*w[2]*w[4]))
End;
```

```
Function /D Thadconvert(int,delt)
variable /D int,delt

variable ans
ans = 1/(int*pi*5.9e6/(3.1*(1+int/3.1 + 4*delt^2)))
ans =ans/3.48e-22/1.1e9
print "conversion factor =", ans
return ans
end;

function ThadFiltermod(in,t,out,tau)
|filters wave in using time constant tau for all t>tau
wave in,out,t
variable tau
variable i=xcsr(B)

out=exp((t-t[xcsr(A)])/tau)*(in*(1+sign(t-t[xcsr(A)]))/2+in[xcsr(A)]
*(1-sign(t-t[xcsr(A)]))/2);
integrate/t out
|out-=out[0]
out*=t[1]-t[0]
out*=exp(-(t-t[xcsr(A)])/tau)/tau
do
out[i] = in[i]
i +=1
```

```
while (i<numpnts(in))


return 0;

end;
```

Bibliography

[Anderson 95] M.H. Anderson, J.R. Ensher, M.R. Matthews, C.E. Wieman, and E. A. Cornell, "Observation of Bose-Einstein condensation in a dilute atomic vapor," Science, **269** 198 (1995).

[Arnold 98] A.S. Arnold, J.S. Wilson, and M.G.Boshier,"A simple extended-cavity diode laser," Rev. Sci. Inst. **69** 1236 (1998).

[Bali 94] S. Bali, D. Hoffmann, T. Walker, "Novel Intensity Dependence of Ultracold Collisions Involving Repulsive States," Europhys. Lett., **27**, 273 (1994).

[Bradley 95] C.C. Bradley, C.A. Sackett, J.J. Tollett, and R.G. Hulet, "Evidence of Bose-Einstein condensation in an atomic gas with attractive interactions," Phys. Rev. Lett., **75** 1687 (1995).

[Burke 97] James P. Burke, Jr., John L. Bohn, B.D. Esry and Chris H. Greene, "Impact of the ^{87}Rb singlet scattering length on suppressing inelastic collisions," Phys. Rev. A **55**, R2511 (1997).

[Chu 85] S. Chu, L. Hollberg, J. Bjorkholm, A. Cable, and A. Ashkin, "Three-dimensional viscous confinement and cooling of atoms by resonance radiation pressure," Phys. Rev. Lett., **55** 48 (1985).

[Chu 86] S. Chu, J. Bjorkholm, A. Cable, and A. Ashkin, "Experimental observation of optically trapped atoms," Phys. Rev. Lett. **57**, 314 (1986).

[Davis 95] K.B. Davis, M.-O. Mewes, M.R. Andrews, N.J. van Druten, D.S. Durfee, D. M. Kurn, and W. Ketterle, "Bose-Einstein condensation in a gas of sodium atoms," Phys. Rev. Lett., **75** 3969 (1995).

[Dineen 92] T. Dineen, C. Wallace, K. Tan, and P. Gould, "Use of trapped atoms to measure absolute photoionization cross sections," Opt. Lett., **17**, 1706 (1992).

[Foot 91] C.J. Foot, "Laser cooling and trapping of atoms," Contemp. Phys. **32**, 369 (1991).

[Gensemer 97] S.D.Gensemer, V. Sanchez-Villicana, K.Y.N. Tan, T.T. Grove, and P.L. Gould, "Trap-loss collisions of ^{85}Rb and ^{87}Rb: Depndence on trap parameters," Phys. Rev. A **56**, 4055 (1997).

[Hoffmann 96] D. Hoffmann, S. Bali, and T. Walker, "Trap-depth measurements using ultracold collisions," Phys. Rev. A, **54** R1030 (1996).

[Julienne 97] P.S. Julienne, F.H. Mies, E. Tiesinga, and C.J. Williams, "Collisional stability of double Bose condensates," Phys. Rev. Lett. **78**, 1880 (1997).

[Kokkelmans 97] S.J.J.M.F. Kokkelmans, H.M.J.M.Boesten, and B.J. Verhaar, "Role of collisions in creation of overlapping Bose condensates," Phys. Rev. A **55**, R1589 (1997).

[Krauss 90] M. Krauss and W.J. Stevens, " Effective core potentials and accurate energy curves for Cs_2 and other alkali diatomics," J. Chem Phys. **93**, 4236 (1990).

[Movre 77] M. Movre and G. Pichler, "Resonance interaction and self-broadening of alkali resonance lines I. Adiabatic potential curves," J. Phys. B. **10**, 2631 (1977).

[Myatt 97] C. J. Myatt, E.A. Burt, R.W. Ghrist, E.A. Cornell, and C.E. Wieman, "Production of two overlapping Bose-Einstein condensates by sympathetic cooling," Phys. Rev. Lett. **78**, 586 (1997).

[Nesnidal 96] R.C. Nesnidal and T.G. Walker, "Multilayer dielectric structure for enhancement of evanescent waves," Appl. Opt. **35**, 2226 (1996).

[Newbury 96] N. Newbury and C. Wieman, "Resource letter TNA-1: Trapping of neutral atoms," Am. J. Phys. **64**, 18 (1996).

[Preston 96] D.W. Preston, "Doppler-free saturated absorption spectroscopy: Laser spectroscopy," Am. J. Phys. **64**, 1432 (1996).

[Raab 87] E. Raab, M. Prentiss, A. Cable, S. Chu, and D. Pritchard, "Trapping of neutralsodium atoms with radiation pressure," Phys. Rev. Lett., **59**, 2631 (1987).

[Sanchez-Villicana 96] V. Sanchez-Villicana, S.D. Gensemer, and P.L. Gould, "Observation of flux enhancement in collision between ultracold atoms," Phys. Rev. A, **54**, R3730 (1996).

[Schappe 95] R.S. Schappe, P. Feng, L.W. Anderson, C.C. Lin, and T.Walker, "Electron collision cross sectionsmeasured with the use of a magneto-optical trap," EuroPhys. Lett **29** 439 (1995).

[Schappe 96] R.S. Schappe, T. Walker, C.C. Lin, and L.W. Anderson, "Abolute electron-impact ionization cross section measurements using a magneto-optical trap," Phys. Rev. Lett. **76**, 4328 (1996).

[Sesko 89] D.Sesko, T. Walker, C. Monroe, A. Gallagher, and C. Wieman, "Collisional losses from a light-force trap," Phys. Rev. Lett. **63** 961 (1989).

[Tiesinga 91] E. Tiesinga, S.J.M. Kuppens, B.J. Verhaar, and H.T.C. Stoof, Phys. Rev. A **43** 5188 (1991).

[Vansteenkiste, 93] N. Vansteenkiste, P. Vignolo, and A. Aspect, "Optical reversibility theorems for polarization: application to remote control of polarization," J. Opt. Soc. Am. A **10**, 2240 (1993).

[Walker 90] T. Walker, D. Sesko, and C. Wieman, "Collective behavior of optically trapped neutral atoms," Phys. Rev. Lett., **64** 408 (1990).

[Wallace 92] C.D. Wallace, T. P. Dineen, K.Y.N. Tan, T.T. Grove, and P.L. Gould, "Isotopic difference in trap loss collisions of laser cooled rubidium atoms," Phys. Rev. Lett. **69** 897 (1992).

[Williams 98] C. Williams, private communication (1998).